Complexation of Alkali and Alkaline Earth Metal Cations by Fluorescent Glycoconjugated Calix[4]arene Derivative: Thermodynamic and Computational Studies

M. Modrušan,[a] N. Cindro,[a]* A. Usenik,[a] K. Leko,[a] L. Glazer,[a] R. Tomaš,[b] G. Horvat,[a] J. Požar,[a] and V. Tomišić[a]*

[a] Department of Chemistry, Faculty of Science, University of Zagreb, Horvatovac 102a, 10000 Zagreb, Croatia
[b] Division of Chemistry, Faculty of Chemistry and Technology, University of Split, Teslina 10/V, 21000 Split, Croatia

SUPPORTING INFORMATION

* Authors to whom correspondence should be addressed. (E-mail addresses: ncindro@chem.pmf.hr, vtomisic@chem.pmf.hr)

Table of Contents

1. Synthetic procedures and characterization

1.1. Synthesis of N-[1,1'-biphenyl]-2-yl-2-chloroacetamide

Commercially available 2-aminobiphenyl (10.0 g, 59.2 mmol) was dissolved in 100 mL of dry DCM after which dry pyridine (9.6 mL, 118.3 mmol) was added and the solution was cooled to 0°C under argon. To a cooled mixture chloroacetyl-chloride (5.0 mL, 62.1 mmol) dissolved in 40 mL of dry DCM was added dropwise throughout 20 minutes. The mixture was stirred for 16 hours at room temperature, then cooled to 0 °C and 100 mL of DCM was added, washed with H_2O (2×200 mL) and saturated $NaHCO_3$ (100 mL). Organic layer was dried over sodium sulfate, filtrated, and DCM was evaporated. The crude solid was dissolved in ethanol, water was added. The crystalized product was filtered and dried in desiccator over P_2O_5 to give 10.9 g (75 %) of pure product.

1.2. Synthesis of 6-(chloromethyl)phenanthridine

N-[1,1'-biphenyl]-2-yl-2-chloroacetamide (10.5 g, 42.7 mmol) was dissolved in $POCl_3$ (39.8 mL, 427 mmol). The mixture was refluxed 21 h at 130 °C with stirring, cooled to cca 40 °C and poured to 1 kg of ice with vigorous stirring until the ice melted. The suspension was filtered and the precipitate was triturated with 100 mL DCM to give 6.0 (53 %) of pure grey product as hydrochloride salt. The reaction mixture filtrate was basified to pH 2 with K_2CO_3 to give white precipitate of product (3.0 g, 31 %) as free base which was filtered and dried in desiccator over P_2O_5.

1.3. Synthesis of 5,11,17,23-tetra-tert-butyl-25,27-bis((phenanthridine-6-yl)methoxy)-26,28-dihydroxycalix[4]arene (P1)

6-(chloromethyl)phenanthridine (2.2 g, 8.3 mmol), NaI (1.2 g, 8.3 mmol), commercially available *p-tert*-butylcalix[4]arene (2.7 g, 4.2 mmol), and potassium carbonate (2.3 g, 16.6 mmol) were suspended in 40 mL of dry acetonitrile. The mixture was refluxed for 3 days at 140 °C with stirring. After removal of acetonitrile the remaining crude solid was suspended in 200 mL DCM and washed with H_2O (100 mL) followed by washing with brine (100 mL). Organic layer was dried over sodium sulfate, filtered, and the solvent was evaporated. The remaining solid was dissolved in small amount of DCM and the propan-2-ol was added. The product that crystalized upon removal of DCM was filtered yielding 1.5 g (35 %) of product.

1.4. Synthesis of bis(2-azidoethyl)amine

Caution! Organic azides are known to explosively decompose. We ran this reaction several times without any unexpected decomposition, but precaution should be taken (*e.g.* face shield and evaporation behind blast shield)

Commercially available bis(2-chloroethyl)amine hydrochloride (7.2 g, 40.3 mmol) was dissolved in 100 mL H_2O after which NaN_3 wad added (13.1 g, 201.7 mmol). The mixture was stirred for 24 h at 90 °C, then cooled and NaOH (w = 30 %) was added until pH 14. The compound was extracted with diethyl ether (3 x 50 mL). Organic layers were combined, washed with brine, and dried over magnesium sulfate. The suspension was filtered and the solvent was evaporated to give 6 g (76 %) of crude bis(2-azidoethyl)amine used without further purification.

1.5. Synthesis of N,N-bis(2-azidoethyl)-2-bromoacetamide

Commercially available bromoacetyl-bromide (3.4 mL, 38.7 mmol) was dissolved in 100 mL of dry DCM and cooled to 0 °C after which the solution of bis(2-azidoethyl)amine (6 g, 38.7 mmol) and DIPEA (6.7 mL, 38.7 mmol) dissolved in 35 mL of dry DCM was added dropwise throughout 10 minutes under argon. The reaction mixture was stirred 16 hours at room temperature and washed with HCl (100 mL, c = 1 mol dm^{-3}), brine (50 mL), and saturated $NaHCO_3$ (50 mL). Organic layer was dried over sodium sulfate, filtered, and the solvent was evaporated to give 9 g of crude product which was purified on column chromatography with silica gel to give 8.7 g (81 %) pure product.

1.6. Synthesis of propargyl-2,3,4,6-tetra-O-acetyl-β-D-glucopyranoside

Prop-2-yn-1-ol (1.8 mL, 30.9 mmol) and α-D-glucose pentaacetate (10.0 g, 25.6 mmol) were dissolved in 100 mL of dry DCM. The mixture was cooled to 0 °C and $BF_3 \times Et_2O$ (18.2 mL, 147.5 mmol) was added dropwise throughout 30 minutes under argon. The solution was stirred over the night at room temperature. The reaction mixture was poured on 200 mL cold brine after which DMC (100 mL) was added. The organic layer was separated and washed with saturated $NaHCO_3$ (100 mL), dried over sodium sulfate, filtered, and the solvent was evaporated. The crude solid was dissolved in ethanol and let to crystalize at low temperature. The crystals were filtered to give 3.83 (32 %) pure product.

1.7. NMR spectra

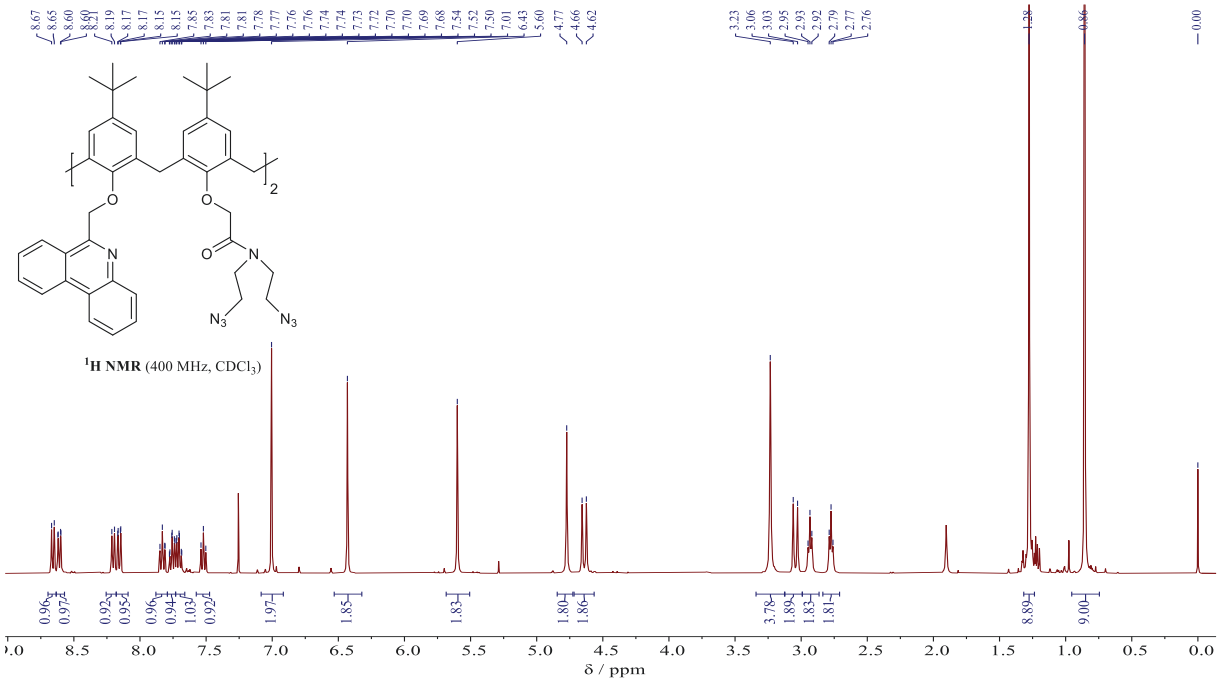

Figure S1. ^{1}H NMR spectrum of **P2** in $CDCl_3$.

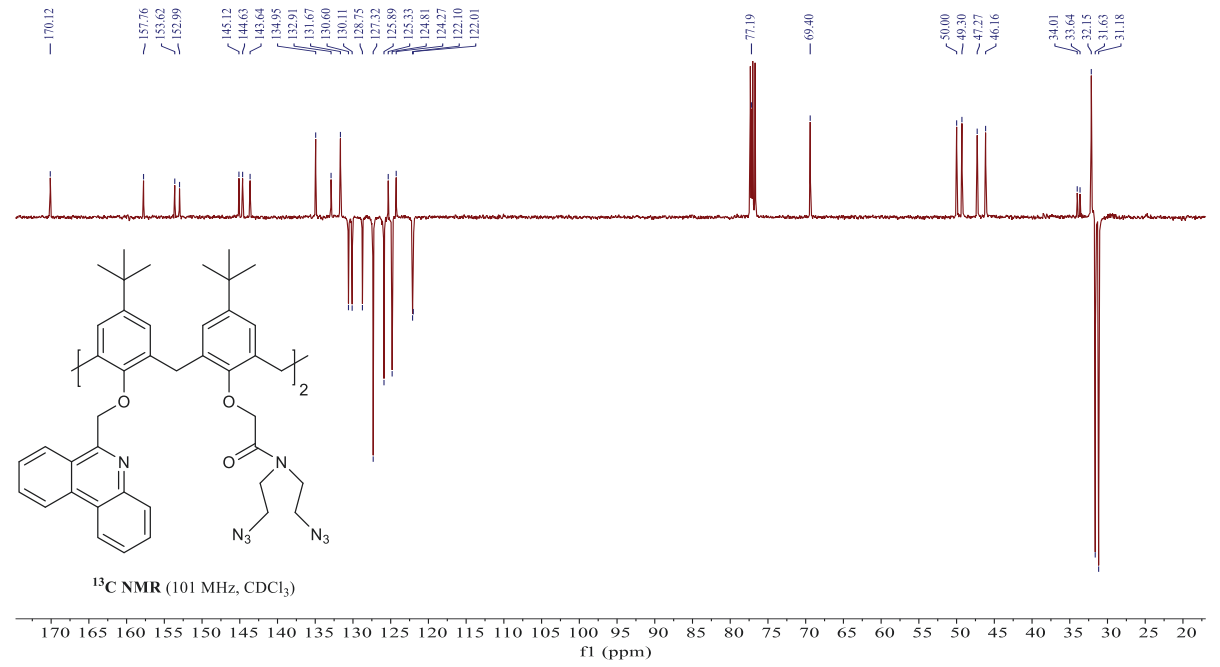

Figure S2. ^{13}C NMR spectrum of **P2** in $CDCl_3$.

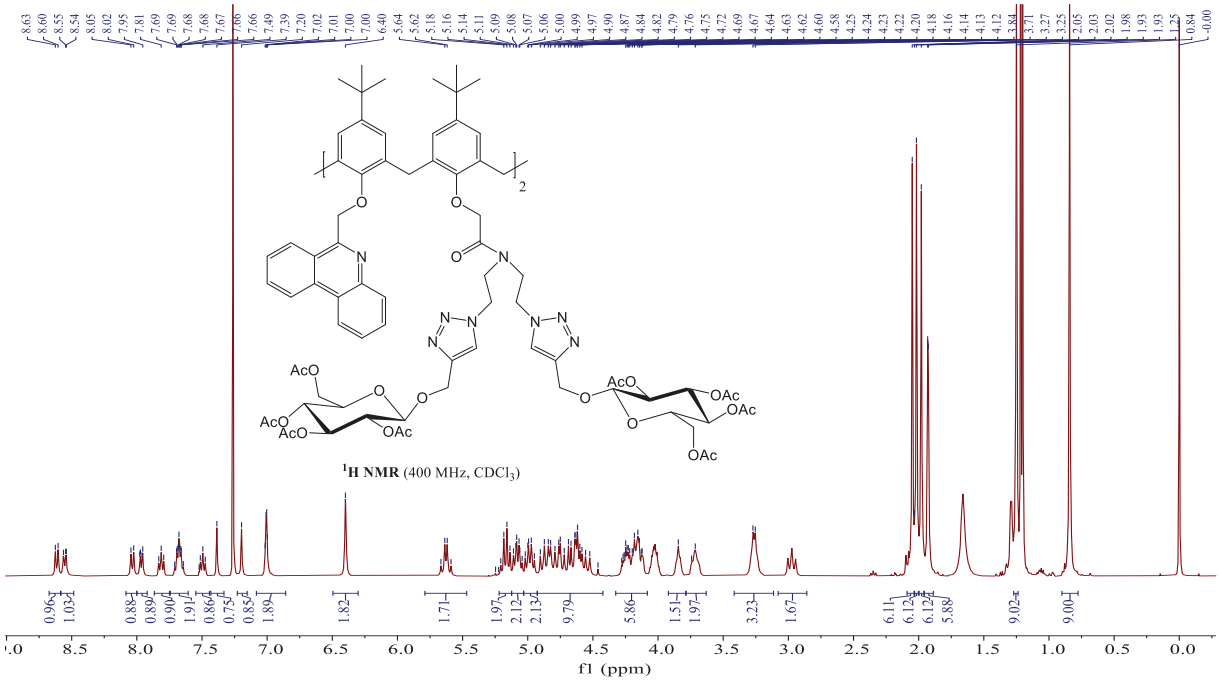

Figure S3. ^{1}H NMR spectrum of **P3** in $CDCl_3$.

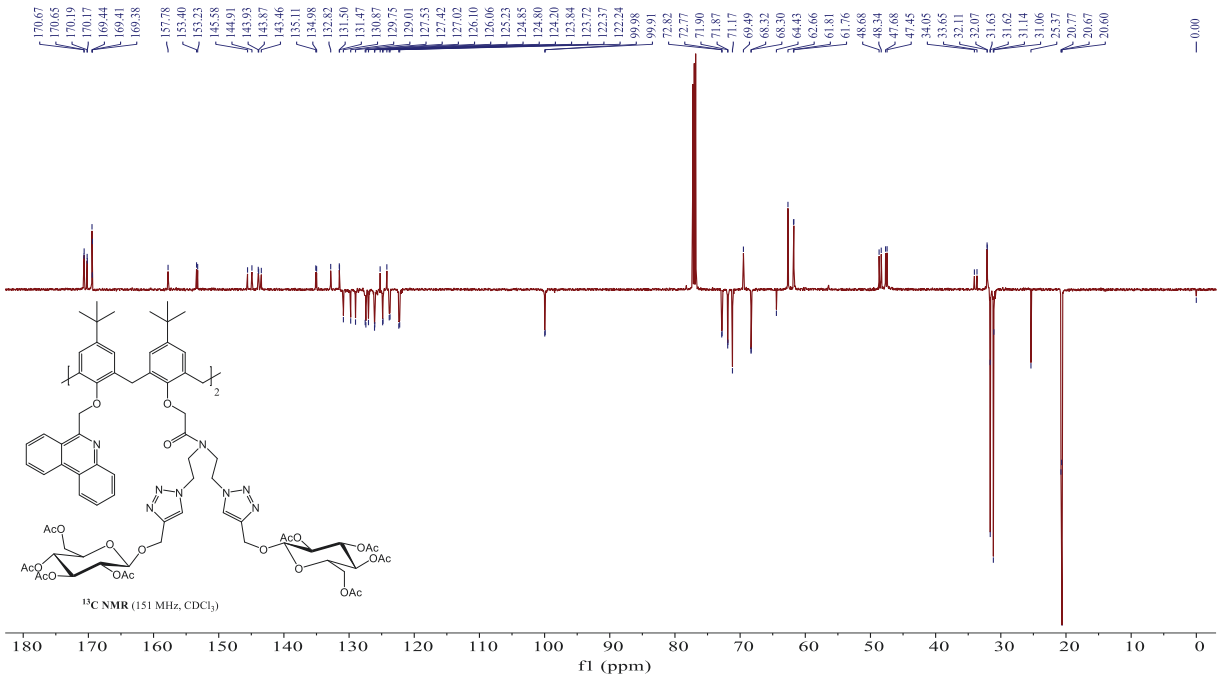

Figure S4. ^{13}C NMR spectrum of **P3** in $CDCl_3$.

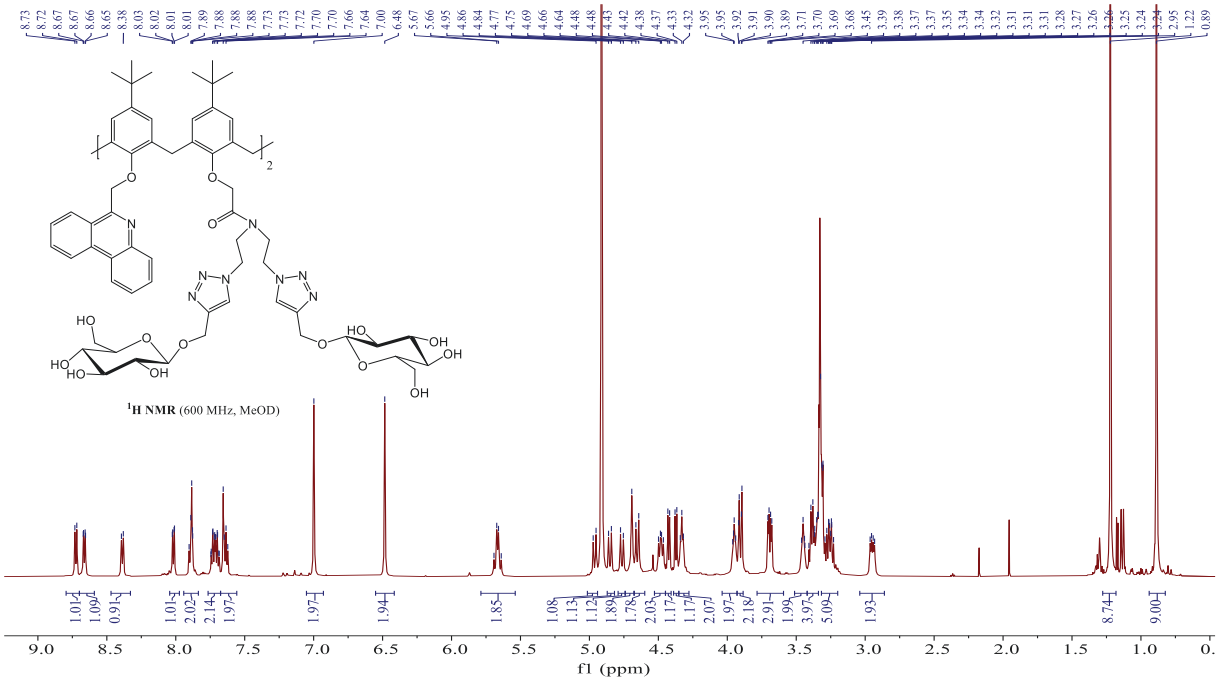

Figure S5. ^{1}H NMR spectrum of **L** in MeOD.

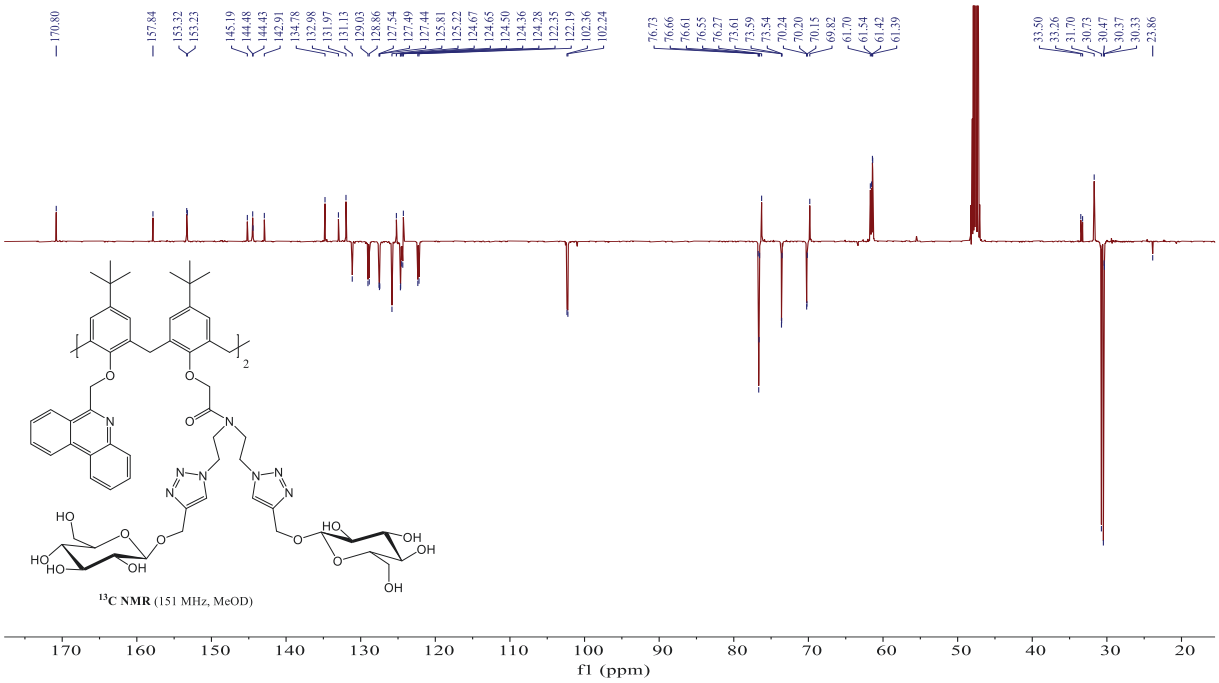

Figure S6. ^{13}C NMR spectrum of **L** in MeOD.

1.8. IR spectra

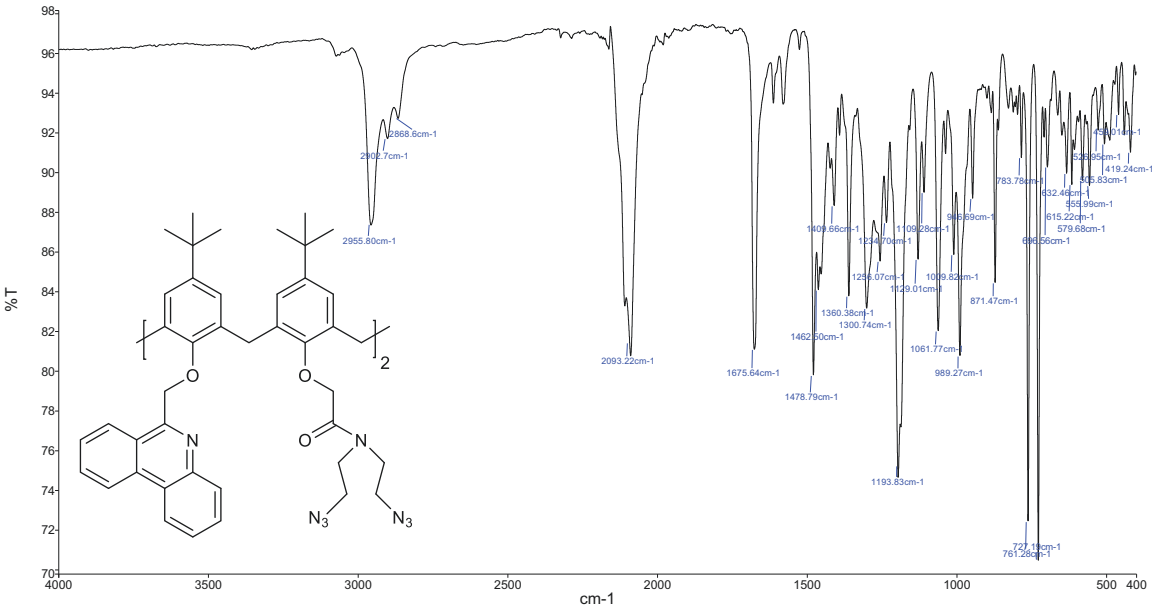

Figure S7. ATR-IR spectrum of **P2**.

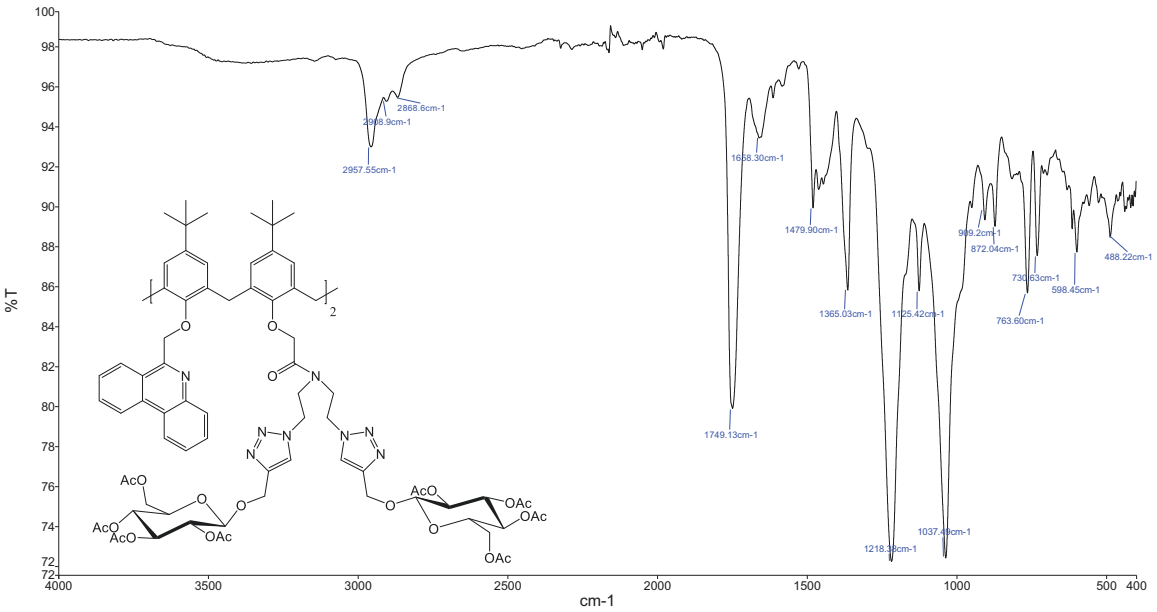

Figure S8. ATR-IR spectrum of **P3**.

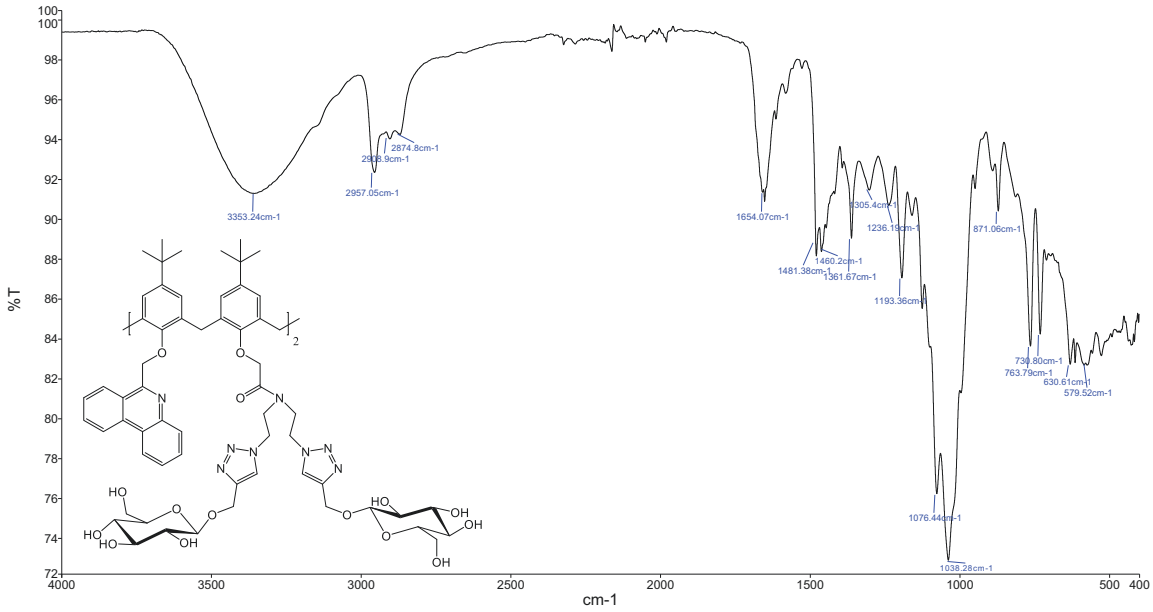

Figure S9. ATR-IR spectrum of **L**.

2. Complexation investigations

2.1. Alkali metal cations

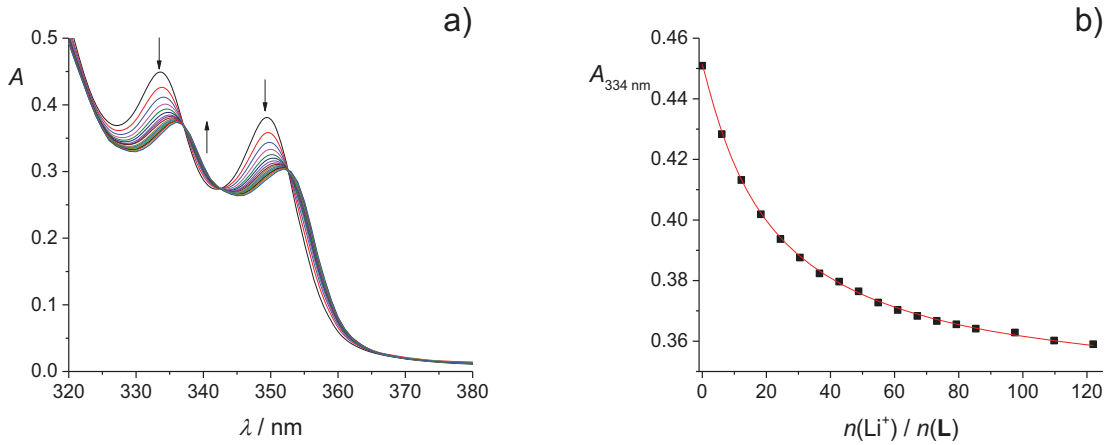

Figure S10. a) Spectrophotometric titration of **L** ($c_0 = 7.54 \times 10^{-5}$ mol dm^{-3}) with $LiClO_4$ ($c = 2.02 \times 10^{-2}$ mol dm^{-3}) in MeOH. $V_0 = 2.2$ mL; $l = 1$ cm; $\vartheta = (25.0 \pm 0.1)$ °C. Spectra are corrected for dilution. b) Absorbance at 334 nm as a function of cation to **L** molar ratio. ■ experimental; – calculated.

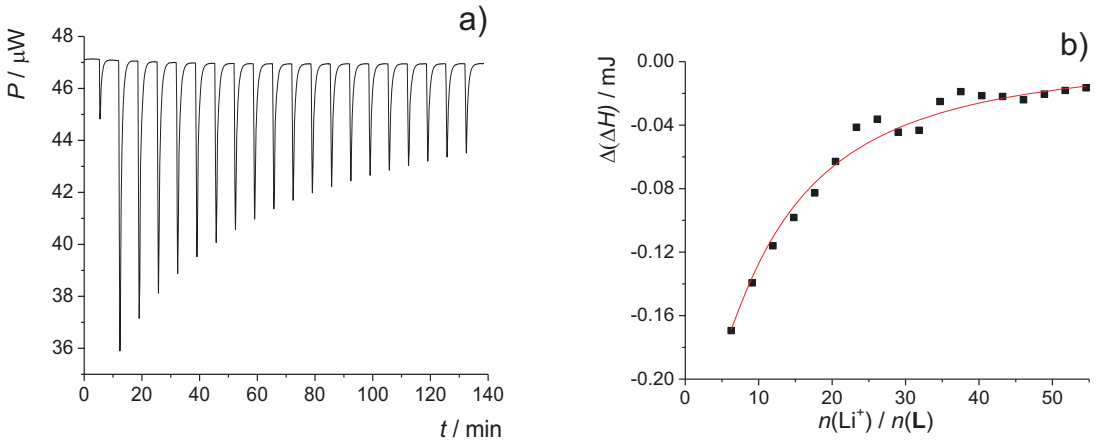

Figure S11. Microcalorimetric titration of **L** ($c_0 = 7.49 \times 10^{-5}$ mol dm^{-3}, $V = 1.43$ cm^3) with $LiClO_4$ ($c = 2.02 \times 10^{-2}$ mol dm^{-3}) in MeOH at 25 °C. a) Thermogram. b) Dependence of successive enthalpy changes on cation to **L** molar ratio. ■ experimental; – calculated.

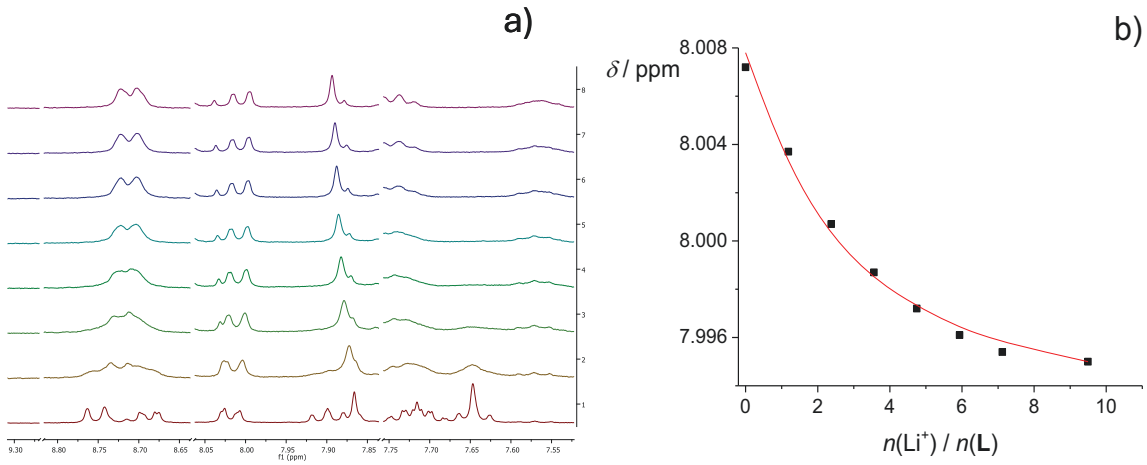

Figure S12. a) ^{1}H NMR titration of **L** (c_0 = 1.42 × 10^{-3} mol dm^{-3}) with $LiClO_4$ (c = 0.15 mol dm^{-3}) in MeOD at 25 °C. b) Chemical shift of phenanthridine protons at 8.01 ppm as a function of cation to **L** molar ratio. ■ experimental; – calculated.

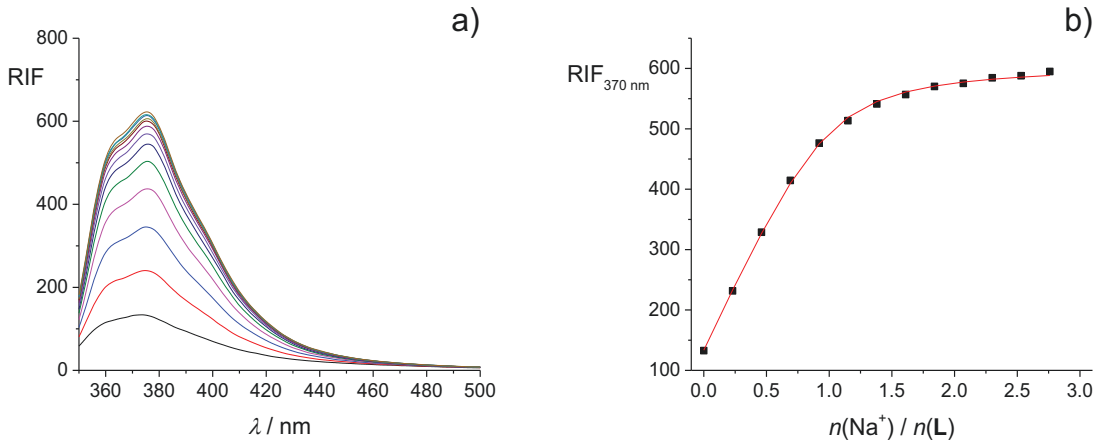

Figure S13. a) Spectrofluorimetric titration of **L** (c_0 = 2.59 × 10^{-5} mol dm^{-3}) with $NaClO_4$ (c = 1.49 × 10^{-3} mol dm^{-3}) in MeOH. V_0 = 2.5 mL; ϑ = (25.0 ± 0.1) °C; λ_{ex} = 330 nm; excitation slit 10 nm; emission slit 10 nm. Spectra are corrected for dilution. b) Relative intensity of fluorescence at 370 nm as a function of cation to **L** molar ratio. ■ experimental; – calculated.

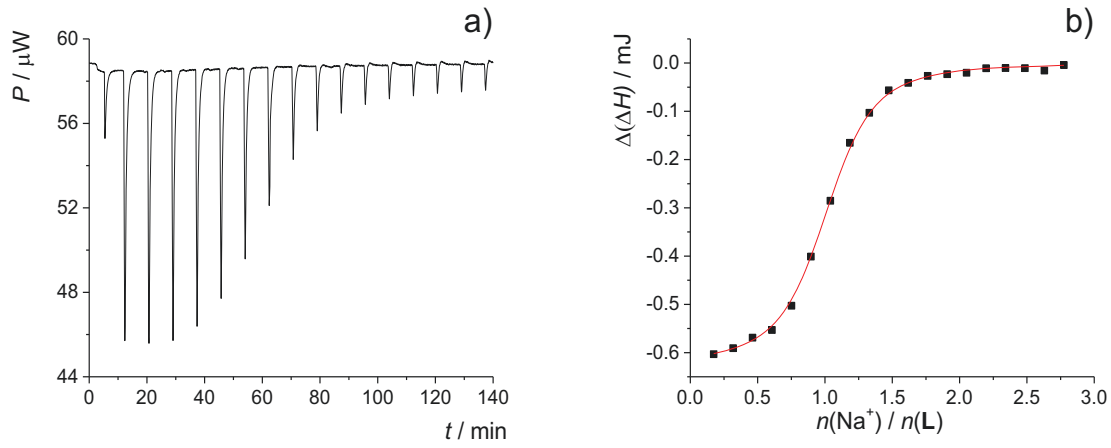

Figure S14. Microcalorimetric titration of **L** (c_0 = 7.34 × 10^{-5} mol dm^{-3}, V = 1.43 cm^3) with $NaClO_4$ (c = 1.01 × 10^{-3} mol dm^{-3}) in MeOH at 25 °C. a) Thermogram. b) Dependence of successive enthalpy changes on cation to **L** molar ratio. ■ experimental; – calculated.

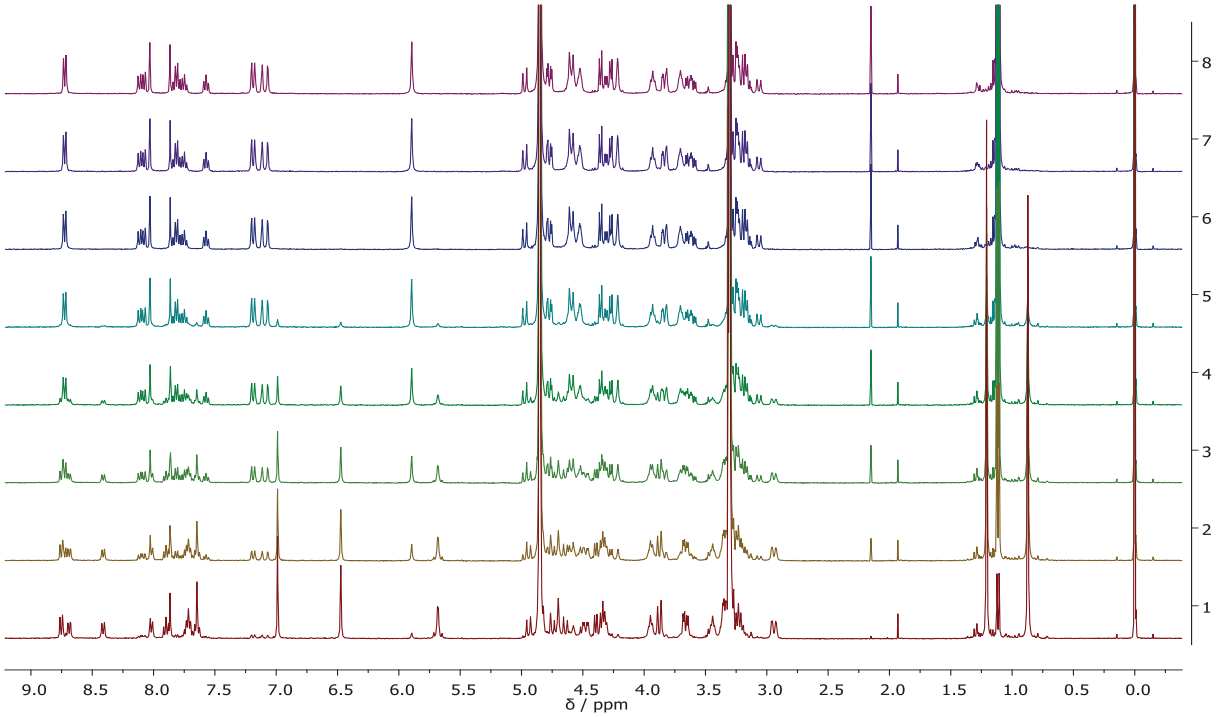

Figure S15. ^{1}H NMR titration of **L** (c_0 = 1.42 × 10^{-3} mol dm^{-3}) with $NaClO_4$ (c = 2.45 × 10^{-2} mol dm^{-3}) in MeOD at 25 °C.

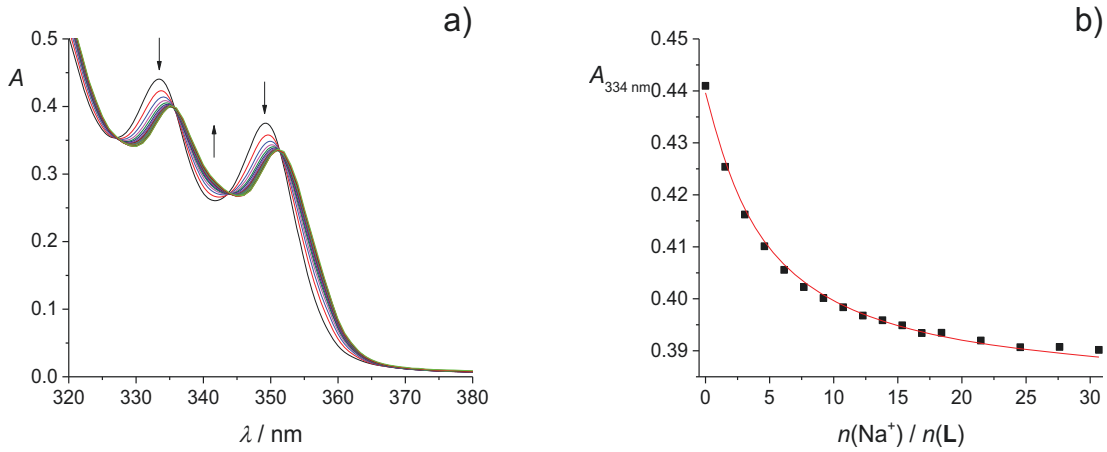

Figure S16. a) Spectrophotometric titration of **L** ($c_0 = 7.54 \times 10^{-5}$ mol dm^{-3}) with $KClO_4$ ($c = 5.09 \times 10^{-3}$ mol dm^{-3}) in MeOH. $V_0 = 2.2$ mL; $l = 1$ cm; $\vartheta = (25.0 \pm 0.1)$ °C. Spectra are corrected for dilution. b) Absorbance at 334 nm as a function of cation to **L** molar ratio. ■ experimental; – calculated.

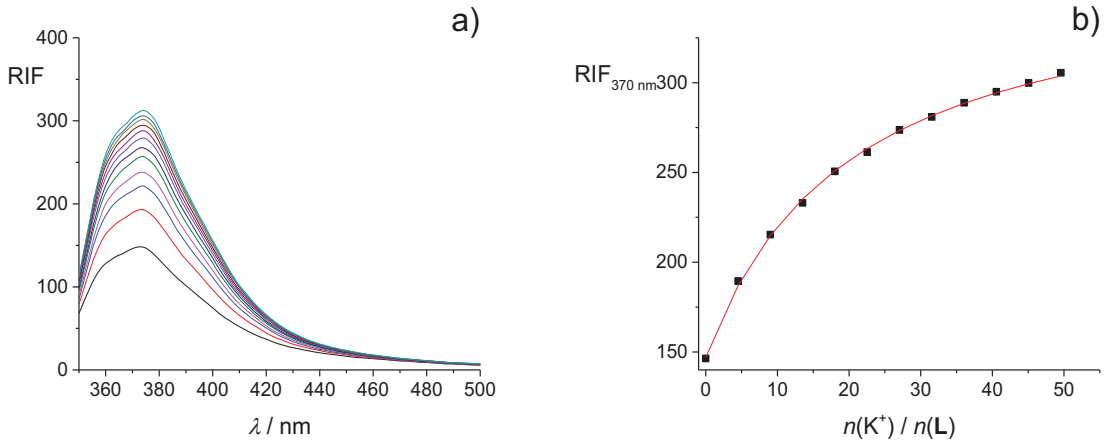

Figure S17. a) Spectrofluorimetric titration of **L** ($c_0 = 2.22 \times 10^{-5}$ mol dm^{-3}) with $KClO_4$ ($c = 5.01 \times 10^{-3}$ mol dm^{-3}) in MeOH. $V_0 = 2.5$ mL; $\vartheta = (25.0 \pm 0.1)$ °C; $\lambda_{ex} = 330$ nm; excitation slit 10 nm; emission slit 10 nm. Spectra are corrected for dilution. b) Relative intensity of fluorescence at 370 nm as a function of cation to **L** molar ratio. ■ experimental; – calculated.

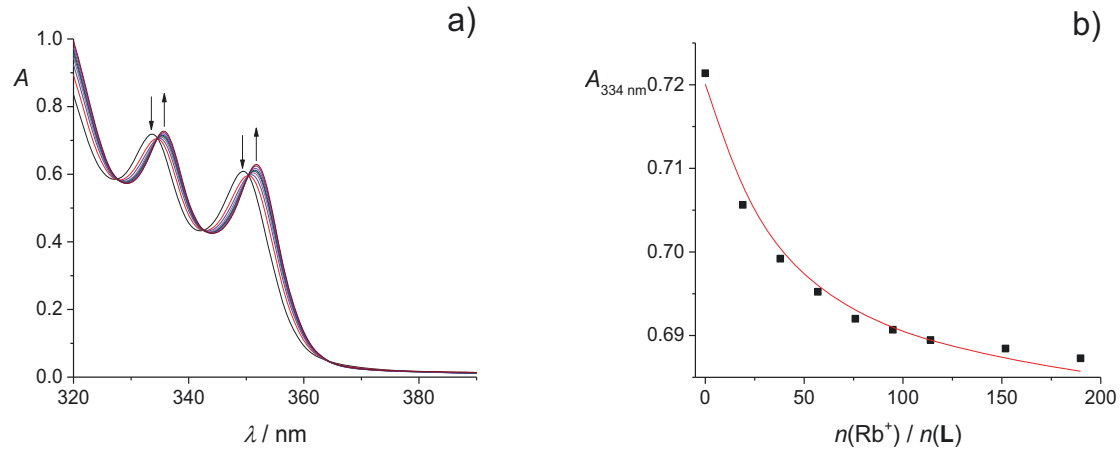

Figure S18. a) Spectrophotometric titration of **L** (c_0 = 1.07 × 10^{-4} mol dm^{-3}) with RbCl (c = 8.91 × 10^{-2} mol dm^{-3}) in MeOH. V_0 = 2.2 mL; l = 1 cm; ϑ = (25.0 ± 0.1) °C. Spectra are corrected for dilution. b) Absorbance at 334 nm as a function of cation to **L** molar ratio. ■ experimental; – calculated.

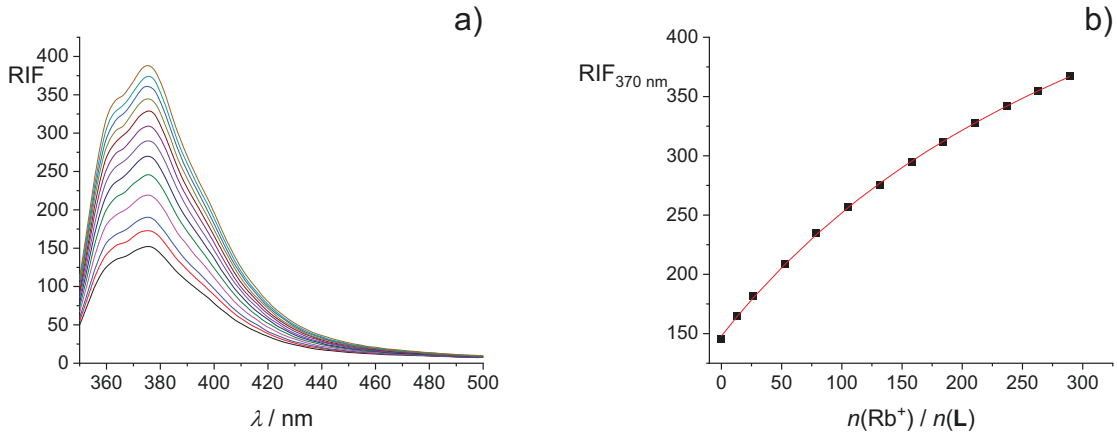

Figure S19. a) Spectrofluorimetric titration of **L** (c_0 = 3.08 × 10^{-5} mol dm^{-3}) with RbCl (c = 2.02 × 10^{-2} mol dm^{-3}) in MeOH. V_0 = 2.5 mL; ϑ = (25.0 ± 0.1) °C; λ_{ex} = 330 nm; excitation slit 10 nm; emission slit 10 nm. Spectra are corrected for dilution. b) Relative intensity of fluorescence at 370 nm as a function of cation to **L** molar ratio. ■ experimental; – calculated.

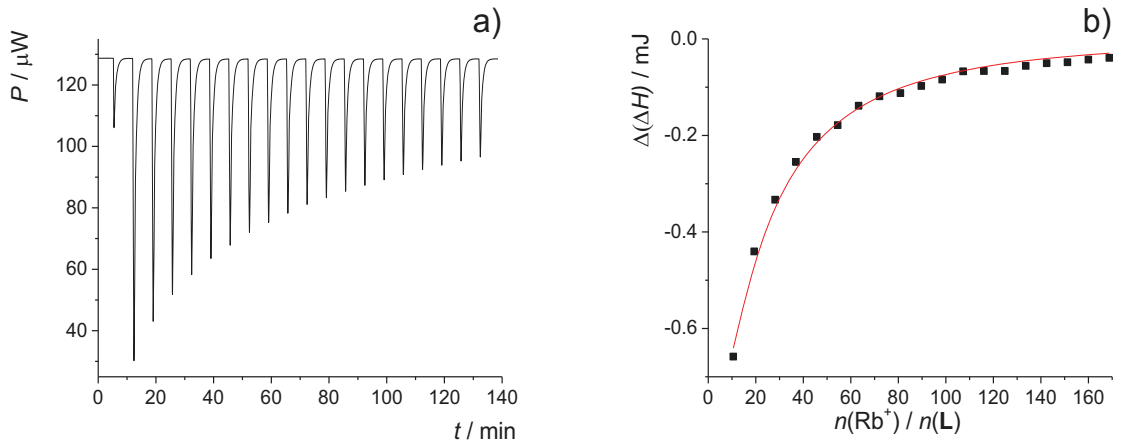

Figure S20. Microcalorimetric titration of **L** (c_0 = 1.07 × 10^{-4} mol dm^{-3}, V = 1.43 cm^3) with RbCl (c = 8.91 × 10^{-2} mol dm^{-3}) in MeOH at 25 °C. a) Thermogram. b) Dependence of successive enthalpy changes on cation to **L** molar ratio. ■ experimental; – calculated.

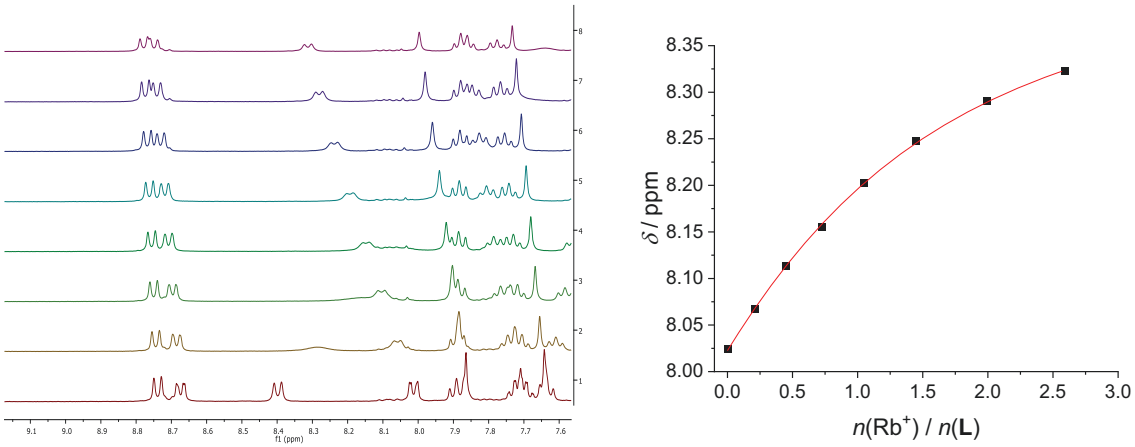

Figure S21. a) ^{1}H NMR titration of **L** (c_0 = 5.15 × 10^{-3} mol dm^{-3}) with RbCl (c = 6.30 × 10^{-2} mol dm^{-3}) in MeOD at 25 °C. b) Chemical shift of phenanthridine protons at 8.02 ppm as a function of cation to **L** molar ratio. ■ experimental; – calculated.

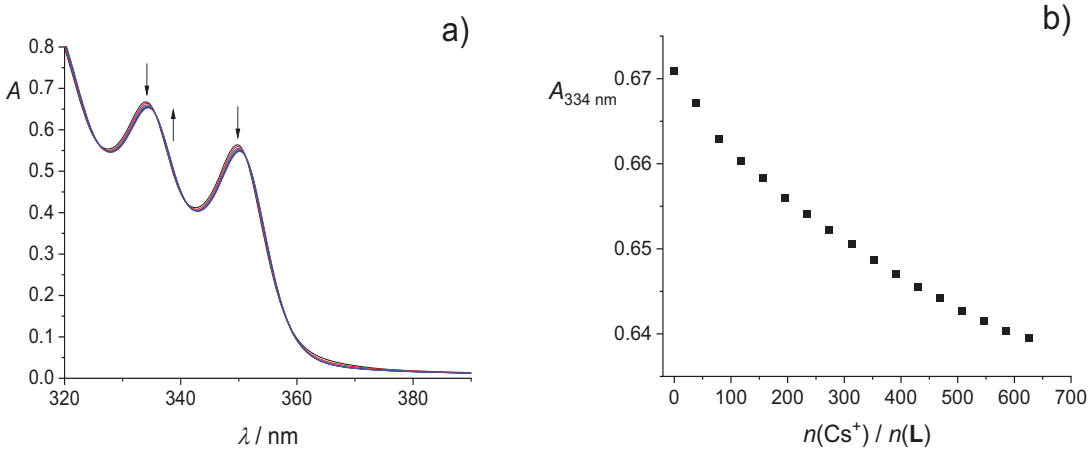

Figure S22. a) Spectrophotometric titration of **L** (c_0 = 1.11 × 10^{-4} mol dm^{-3}) with CsCl (c = 0.11 mol dm^{-3}) in MeOH. V_0 = 2.2 mL; l = 1 cm; ϑ = (25.0 ± 0.1) °C. Spectra are corrected for dilution. b) Absorbance at 334 nm as a function of cation to **L** molar ratio. ■ experimental; – calculated.

2.2. Alkaline earth metal cations

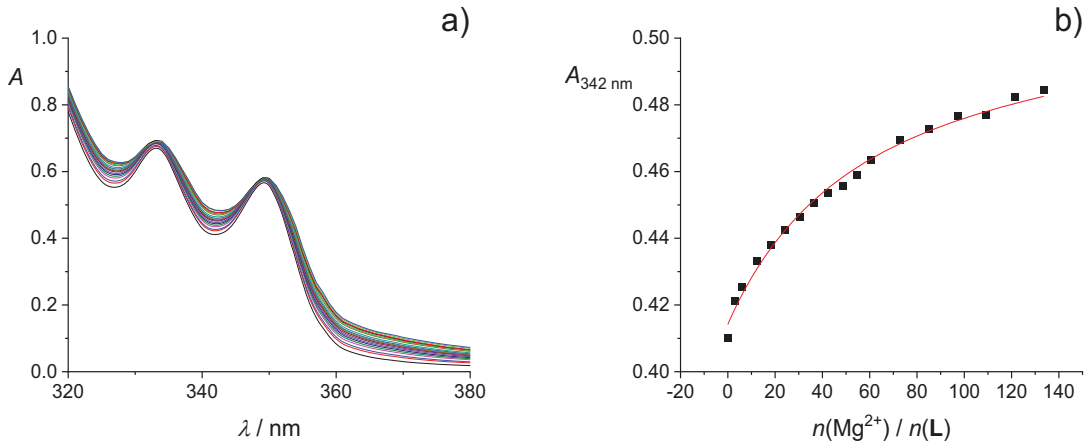

Figure S23. a) Spectrophotometric titration of **L** ($c_0 = 1.55 \times 10^{-4}$ mol dm^{-3}) with $Mg(ClO_4)_2$ ($c = 4.14 \times 10^{-2}$ mol dm^{-3}) in MeOH. $V_0 = 2.2$ mL; $l = 1$ cm; $\vartheta = (25.0 \pm 0.1)$ °C. Spectra are corrected for dilution. b) Absorbance at 342 nm as a function of cation to **L** molar ratio. ■ experimental; – calculated.

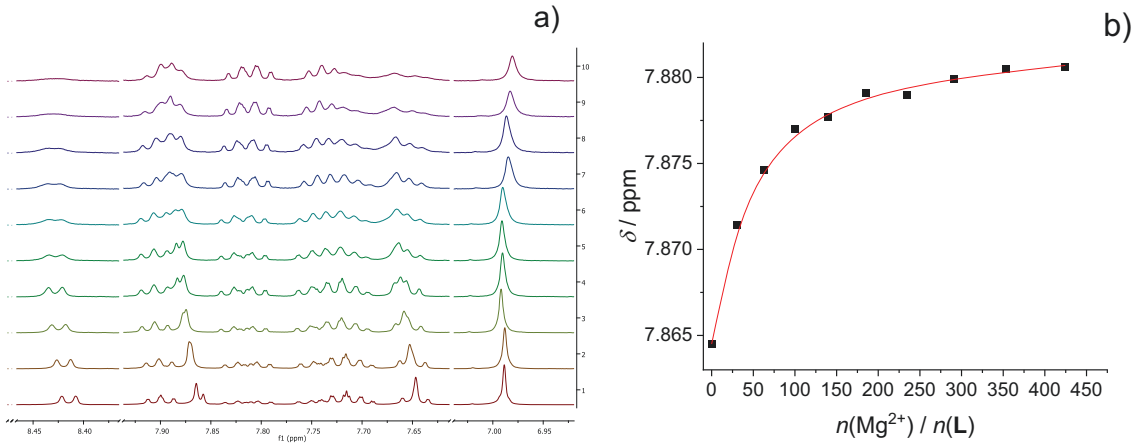

Figure S24. a) ^{1}H NMR titration of **L** ($c_0 = 1.65 \times 10^{-4}$ mol dm^{-3}) with $Mg(ClO_4)_2$ ($c = 0.10$ mol dm^{-3}) in MeOD. b) Chemical shift of triazole protons at 7.86 ppm as a function of cation to **L** molar ratio. ■ experimental; – calculated.

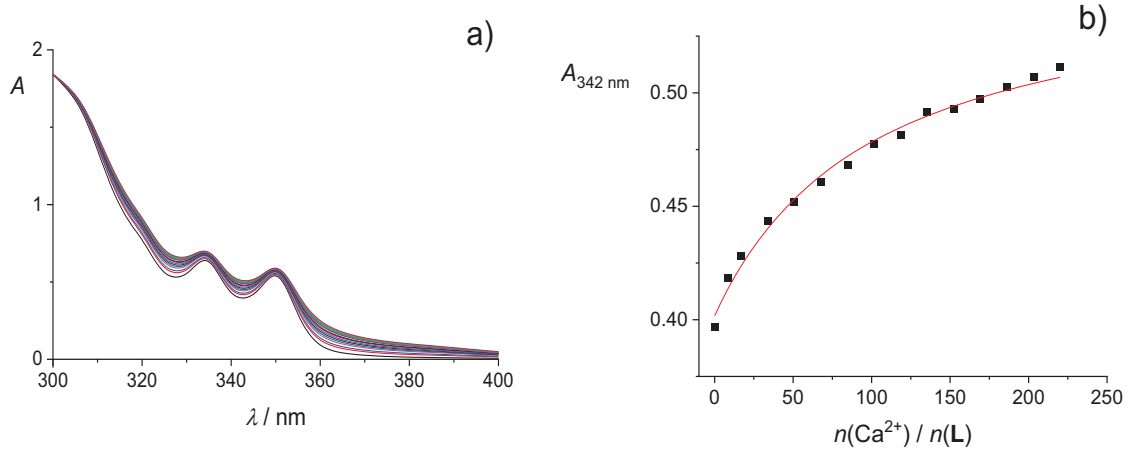

Figure S25. a) Spectrophotometric titration of **L** (c_0 = 1.50 × 10^{-4} mol dm^{-3}) with $Ca(ClO_4)_2$ (c = 0.11 mol dm^{-3}) in MeOH. V_0 = 2.2 mL; l = 1 cm; ϑ = (25.0 ± 0.1) °C. Spectra are corrected for dilution. b) Absorbance at 342 nm as a function of cation to **L** molar ratio. ■ experimental; – calculated.

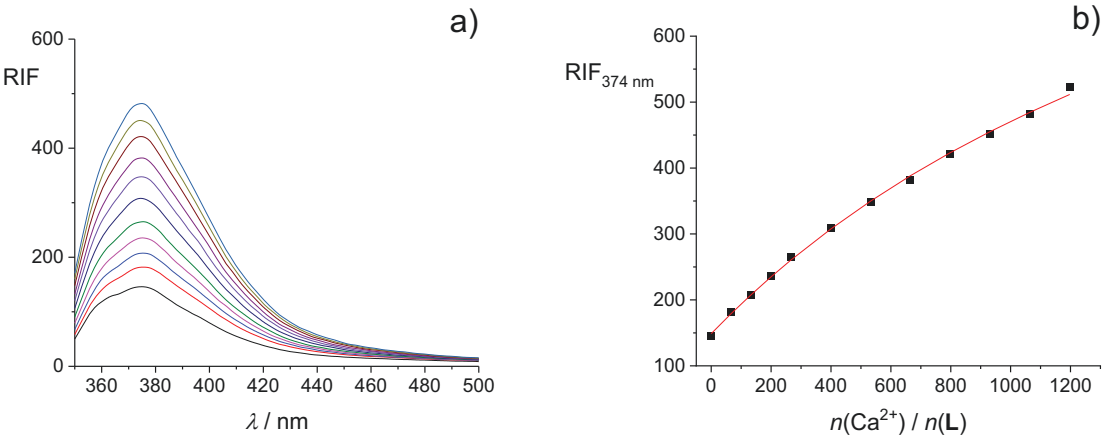

Figure S26. a) Spectrofluorimetric titration of **L** (c_0 = 3.41 × 10^{-5} mol dm^{-3}) with $Ca(ClO_4)_2$ (c = 9.98 × 10^{-2} mol dm^{-3}) in MeOH. V_0 = 2.5 mL; ϑ = (25.0 ± 0.1) °C; λ_{ex} = 330 nm; excitation slit 10 nm; emission slit 10 nm. Spectra are corrected for dilution. b) Relative intensity of fluorescence at 376 nm as a function of cation to **L** molar ratio. ■ experimental; – calculated.

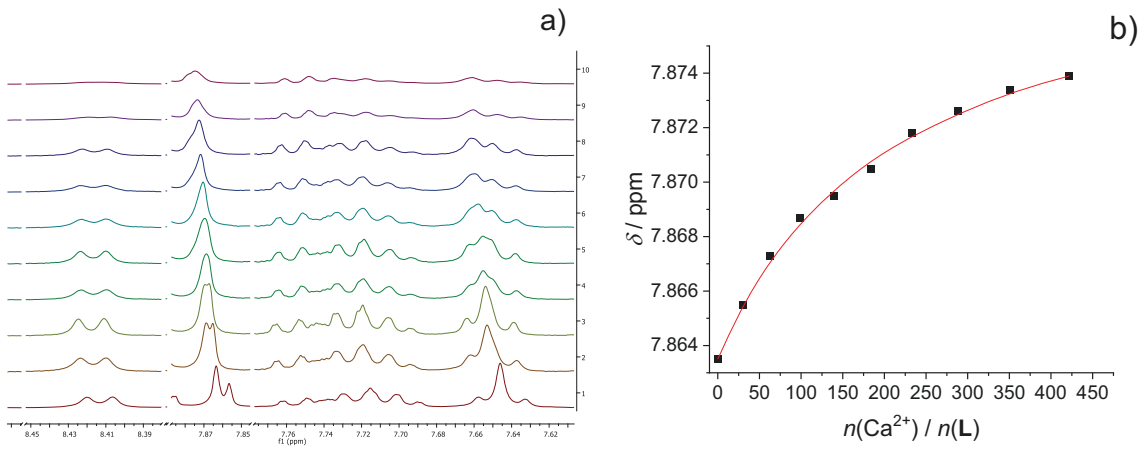

Figure S27. a) ^{1}H NMR titration of **L** (c_0 = 1.57 × 10^{-4} mol dm^{-3}) with $Ca(ClO_4)_2$ (c = 0.10 mol dm^{-3}) in MeOD. b) Chemical shift of triazole protons at 7.86 ppm as a function of cation to **L** molar ratio. ■ experimental; – calculated.

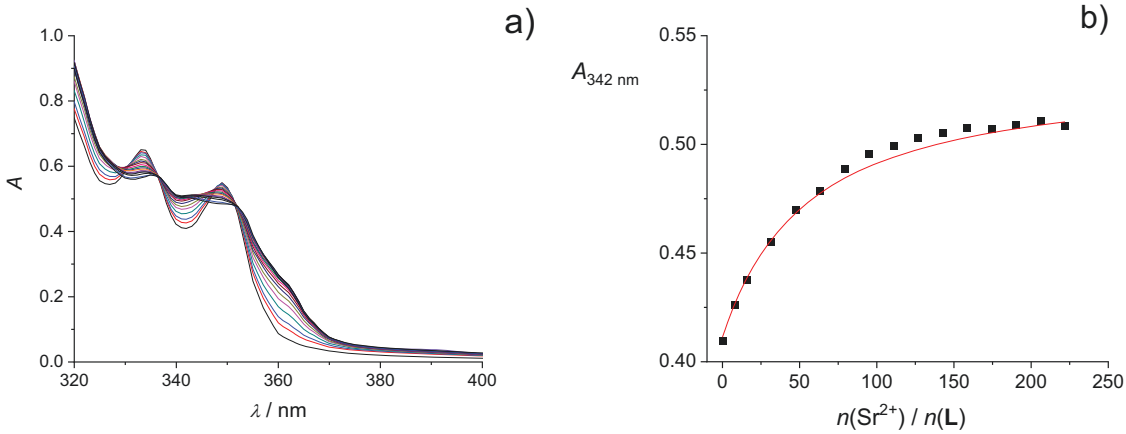

Figure S28. a) Spectrophotometric titration of **L** (c_0 = 1.50 × 10^{-4} mol dm^{-3}) with $Sr(ClO_4)_2$ (c = 0.11 mol dm^{-3}) in MeOH. V_0 = 2.2 mL; l = 1 cm; ϑ = (25.0 ± 0.1) °C. Spectra are corrected for dilution. b) Absorbance at 342 nm as a function of cation to **L** molar ratio. ■ experimental; – calculated.

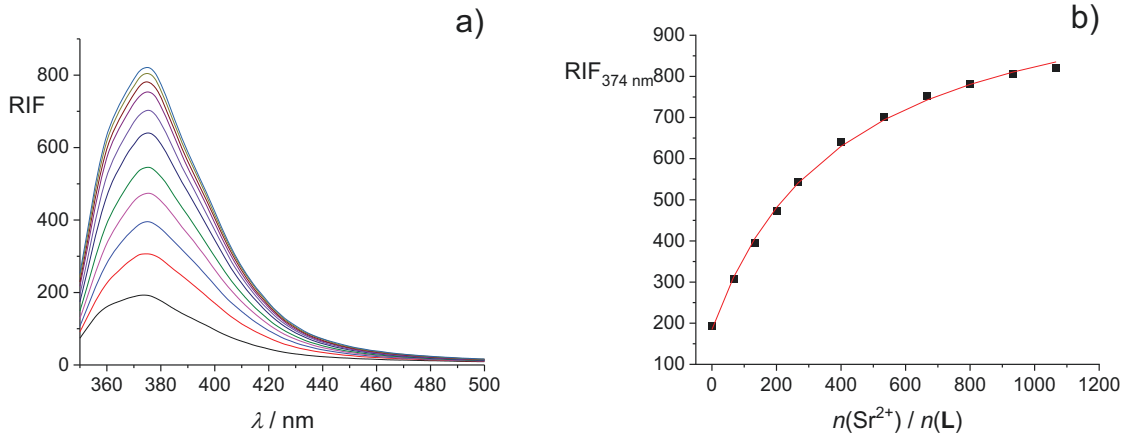

Figure S29. a) Spectrofluorimetric titration of **L** (c_0 = 3.41 × 10^{-5} mol dm^{-3}) with $Sr(ClO_4)_2$ (c = 0.10 mol dm^{-3}) in MeOH. V_0 = 2.5 mL; ϑ = (25.0 ± 0.1) °C; λ_{ex} = 330 nm; excitation slit 10 nm; emission slit 10 nm. Spectra are corrected for dilution. b) Relative intensity of fluorescence at 374 nm as a function of cation to **L** molar ratio. ■ experimental; – calculated.

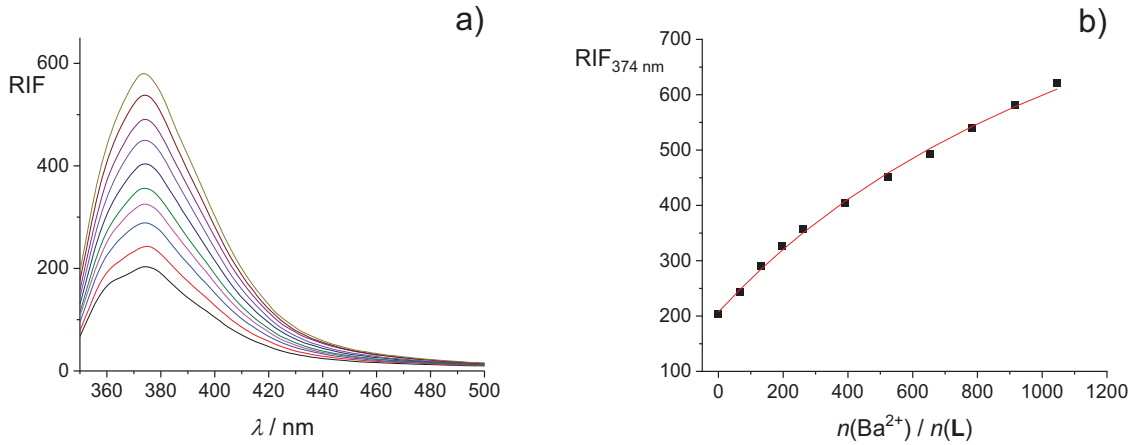

Figure S30. a) Spectrofluorimetric titration of **L** (c_0 = 3.48 × 10^{-5} mol dm^{-3}) with $Ba(ClO_4)_2$ (c = 0.10 mol dm^{-3}) in MeOH. V_0 = 2.5 mL; ϑ = (25.0 ± 0.1) °C; λ_{ex} = 330 nm; excitation slit 10 nm; emission slit 10 nm. Spectra are corrected for dilution. b) Relative intensity of fluorescence at 374 nm as a function of cation to **L** molar ratio. ■ experimental; – calculated.

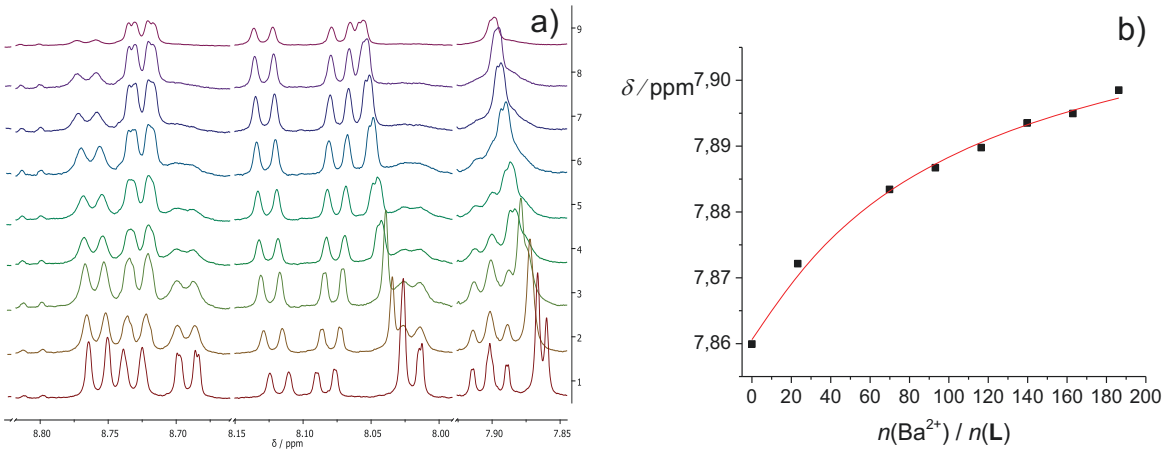

Figure S31. a) ^{1}H NMR titration of **L** (c_0 = 1.72 × 10^{-4} mol dm^{-3}) with $Ba(ClO_4)_2$ (c = 0.10 mol dm^{-3}) in MeOD. b) Chemical shift of triazole protons at 7.86 ppm as a function of cation to **L** molar ratio. ■ experimental; – calculated.

3. Molecular dynamics simulations

3.1. Alkali metal cations

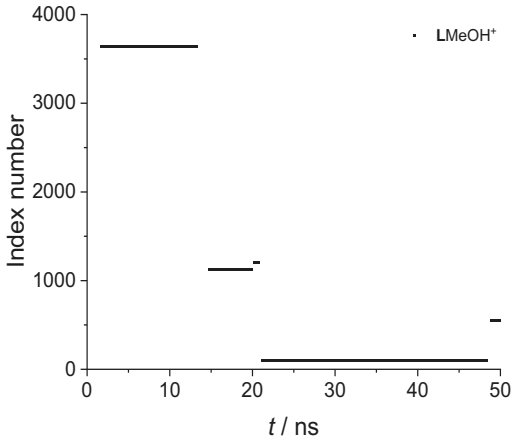

Figure S32. Index number of methanol that occupy hydrophobic cavity of **L**MeOH$^+$ during MD simulations in methanol at 25 °C.

Table S1. Energies of interactions of **L** with solvent molecules, occurrence time ratio of different chemical species, and the structure of calixarene *basket* obtained by MD simulations in methanol at 25 °C.

	MeOH	
	LMeOH	**L**
E(**L**–MeOH) / kJ mol^{-1}	–1497	–1395
E(**L**–MeOH$_{incl}$) / kJ mol^{-1}	–42	/
t_{total} / ns	50	
t / t_{total}	0.915	0.085
N(MeOH$_{incl}$)	5	/
$\overline{d}$ / Å	7.67	6.79
	7.89	8.34
σ(d) / Å	0.26	0.65
	0.25	0.50
$\lvert d - d_{ref}\rvert$ / Å	0.25	1.09
	0.21	0.60

$\overline{d}$ denotes average distance between opposing aryl carbon atoms connected to the *tert*-butyl groups and d_{ref} = 7.85 Å corresponds to C_{4v} *cone* conformation.

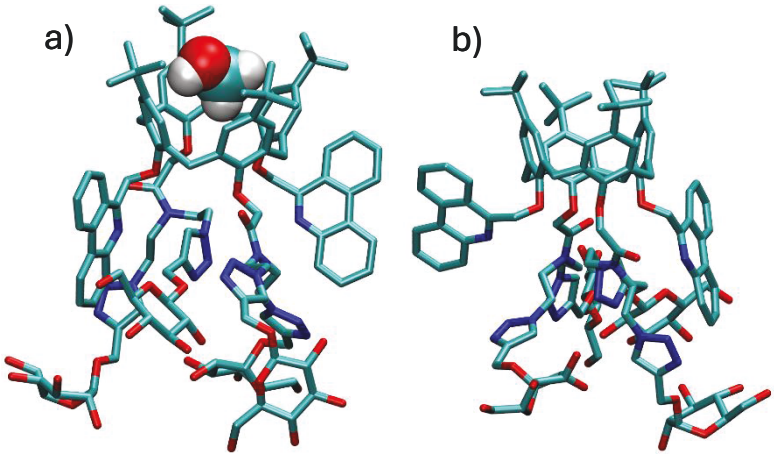

Figure S33. Representative structures of a) **L**MeOH adduct and b) free **L** obtained by MD simulations at 25 °C. Hydrogen atoms of **L** are omitted for clarity.

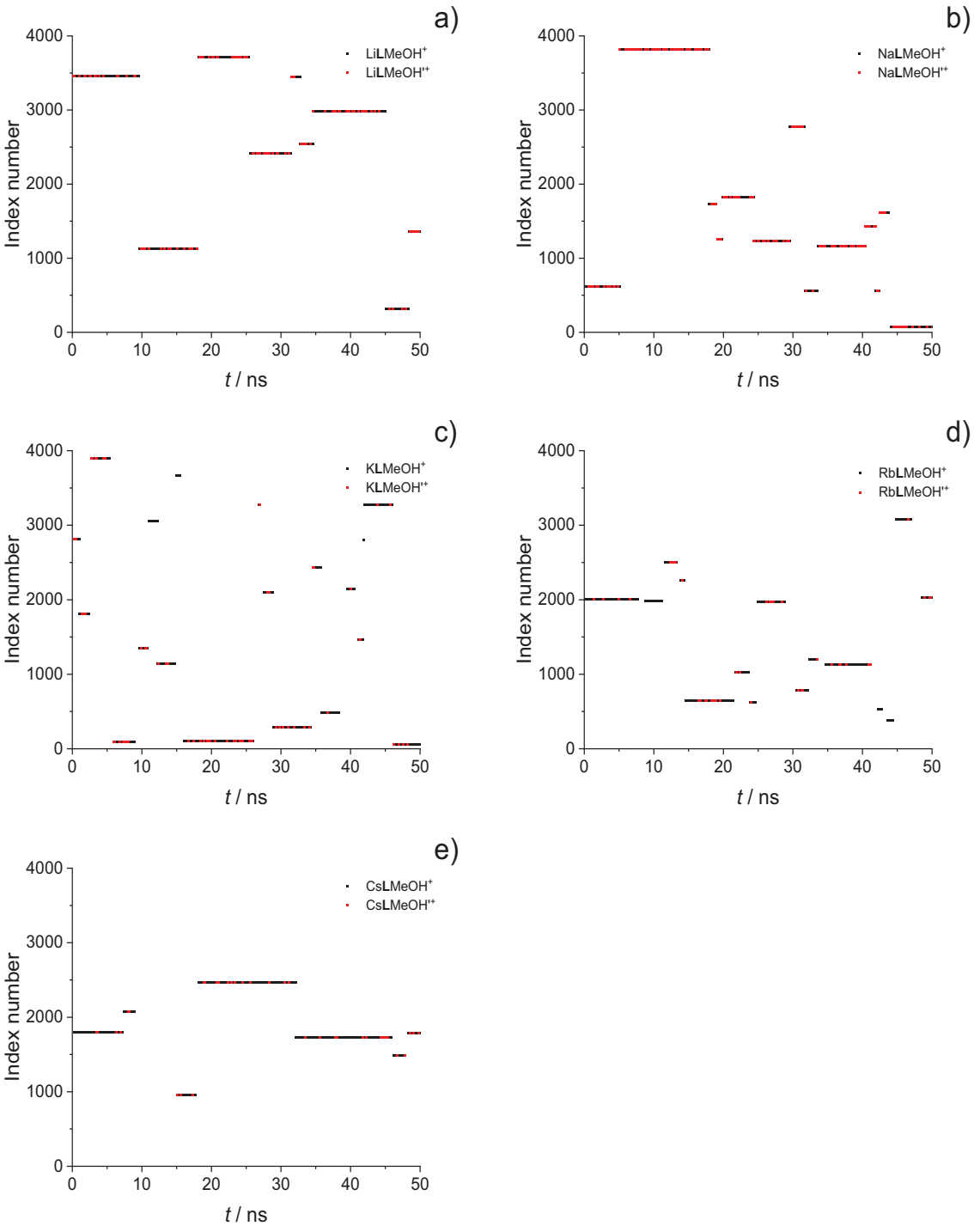

Figure S34. Index number of methanol that occupy hydrophobic cavities of a) Li**L**MeOH$^+$ and Li**L**MeOH'$^+$, b) Na**L**MeOH$^+$ and Na**L**MeOH'$^+$, c) K**L**MeOH$^+$ and K**L**MeOH'$^+$, d) Rb**L**MeOH$^+$ and Rb**L**MeOH'$^+$, e) Ba**L**MeOH$^+$ and Ba**L**MeOH'$^+$ during MD simulations in methanol at 25 °C.

Table S2. Energies of interactions of **L** with lithium, sodium, potassium, rubidium, and cesium cations in methanol, occurrence time ratio of different chemical species, the number of ether, carbonyl, phenanthridine, and triazole groups which coordinate metal cations, and the structure of calixarene basket in the complexes obtained by MD simulations in methanol at 25 °C.

	Li^+			Na^+			K^+		
	Li**L**MeOH$^+$	Li**L**MeOH'$^+$	Li**L**$^+$	Na**L**MeOH$^+$	Na**L**MeOH'$^+$	Na**L**$^+$	K**L**MeOH$^+$	K**L**MeOH'$^+$	K**L**$^+$
E(M$^+$–**L**) / kJ mol^{-1}	–557	–548	–544	–480	–478	–479	–402	–383	–399
E(**L**–MeOH) / kJ mol^{-1}	–1661	–1652	–1601	–1506	–1480	–1414	–1599	–1596	–1543
E(**L**–MeOH$_{incl}$) / kJ mol^{-1}	–47	–33	/	–48	–31	/	–49	–38	/
E(M$^+$–MeOH) / kJ mol^{-1}	–3	–12	–11	4	–11	–3	3	–2	–3
E(M$^+$–MeOH$_{incl}$) / kJ mol^{-1}	7	–4	/	7	–9	/	5	–4	/
t_{total} / ns		50			50				
t / t_{total}	0.970	0.009	0.021	0.952	0.023	0.025	0.852	0.005	0.143
N(coord., C–O–C)	3.09	3.21	3.08	3.86	3.91	3.87	3.58	3.66	3.57
N(coord., C=O)	1.98	1.86	1.85	1.95	1.91	1.95	1.79	1.46	1.86
N(coord., N_{phen})	0.00	0.00	0.00	0.00	0.00	0.00	0.76	0.54	0.69
N(coord., N_{triaz})	0.00	0.00	0.00	0.00	0.00	0.00	0.10	0.37	0.04
N(MeOH$_{incl}$)	9	9	/	13	13	/	19	16	/
$\overline{d}$ / Å	7.96 8.01	7.93 8.06	7.57 8.21	8.06 7.87	8.02 7.88	8.14 7.59	8.02 7.70	7.95 7.75	8.33 7.03
σ(d) / Å	0.29 0.28	0.33 0.31	0.59 0.49	0.28 0.27	0.28 0.27	0.40 0.45	0.29 0.28	0.36 0.37	0.62 0.69
$\lvert d - d_{ref}\rvert$ / Å	0.25 0.26	0.27 0.31	0.50 0.50	0.28 0.22	0.26 0.22	0.41 0.41	0.27 0.26	0.30 0.31	0.67 0.94

	Rb^+			Cs^+		
	Rb**L**MeOH$^+$	Rb**L**MeOH'$^+$	Rb**L**$^{2+}$	Cs**L**MeOH$^+$	Cs**L**MeOH'$^+$	Cs**L**$^+$
E(M$^+$–**L**) / kJ mol^{-1}	–327	–326	–324	–297	–298	–305
E(**L**–MeOH) / kJ mol^{-1}	–1674	–1688	–1646	–1740	–1747	–1694
E(**L**–MeOH$_{incl}$) / kJ mol^{-1}	–52	–37	/	–45	–35	/
E(M$^+$–MeOH) / kJ mol^{-1}	–23	–24	–28	–22	–25	–14
E(M$^+$–MeOH$_{incl}$) / kJ mol^{-1}	5	–4	/	4	1	/
t_{total} / ns		50			50	
t / t_{total}	0.781	0.003	0.216	0.839	0.002	0.159
N(coord., C–O–C)	3.82	3.93	3.80	3.78	3.76	3.77
N(coord., C=O)	1.86	1.96	1.93	1.71	1.85	1.89
N(coord., N_{phen})	0.95	0.84	0.94	1.19	1.34	1.50
N(coord., N_{triaz})	0.05	0.00	0.00	0.19	0.03	0.00
N(MeOH$_{incl}$)	15	12	/	7	7	/
/ Å	7.95 7.71	7.91 7.73	8.37 6.92	7.96 7.68	8.04 7.65	8.58 6.58
σ(d) / Å	0.28 0.27	0.31 0.31	0.50 0.62	0.27 0.27	0.26 0.27	0.43 0.57
$\lvert d - d_{ref}\rvert$ / Å	0.23 0.25	0.26 0.27	0.63 0.97	0.24 0.26	0.27 0.28	0.77 1.28

$\overline{d}$ denotes average distance between opposing aryl carbon atoms connected to the *tert*-butyl groups and d_{ref} = 7.85 Å corresponds to C_{4v} *cone* conformation.

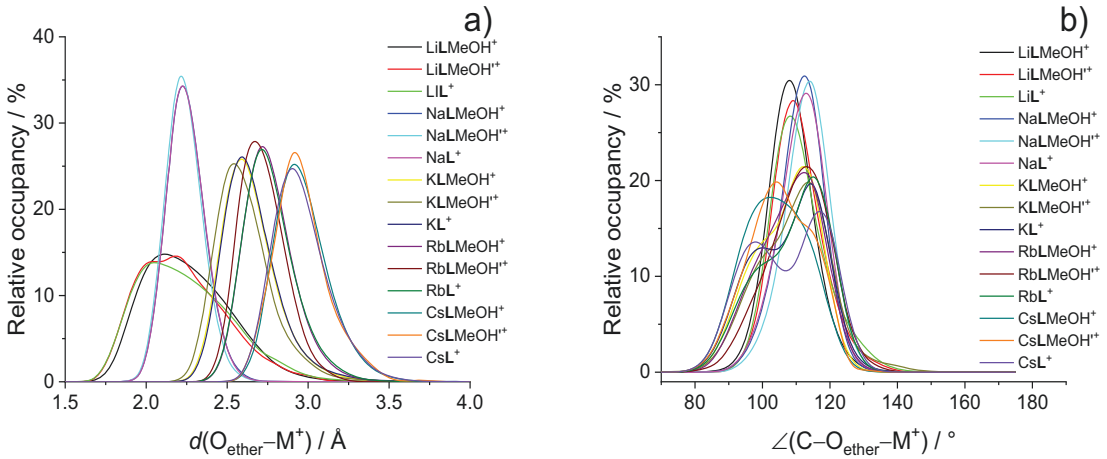

Figure S35. Distribution of a) metal cation–ether oxygen distances and b) metal cation–ether oxygen angles for M^+–**L** complexes in methanol obtained by MD simulations. Data was binned at 0.1 Å and 5 ° interval, respectively.

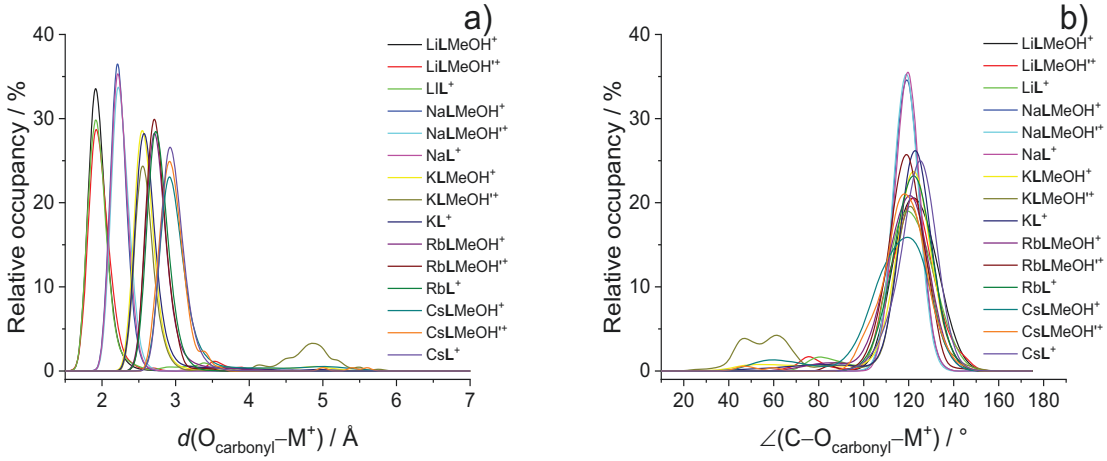

Figure S36. Distribution of a) metal cation–carbonyl oxygen distances and b) metal cation–carbonyl oxygen angles for M^+–**L** complexes in methanol obtained by MD simulations. Data was binned at 0.1 Å and 5 ° interval, respectively.

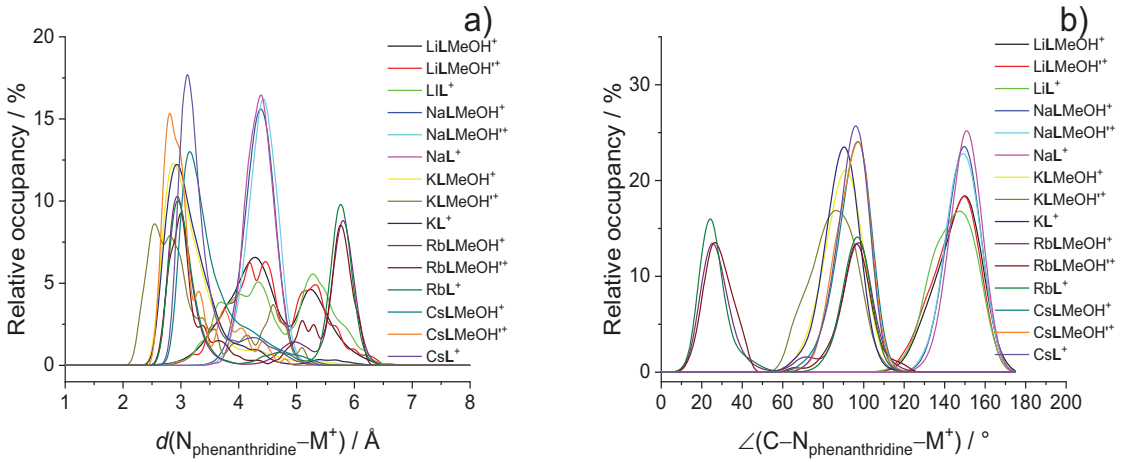

Figure S37. Distribution of a) metal cation–phenanthridine nitrogen distances and b) metal cation–phenanthridine nitrogen angles for M^+–**L** complexes in methanol obtained by MD simulations. Data was binned at 0.1 Å and 5 ° interval, respectively.

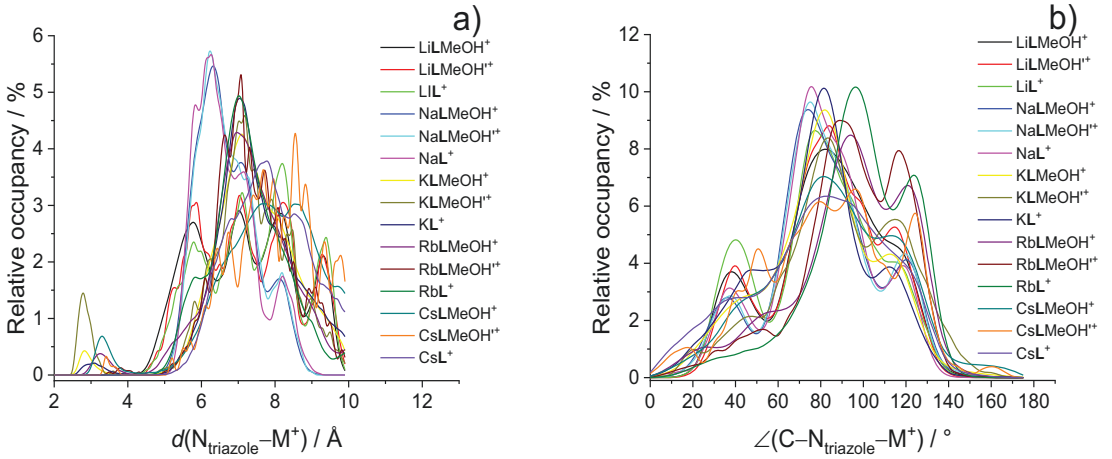

Figure S38. Distribution of a) metal cation–triazole nitrogen distances and b) metal cation–triazole nitrogen angles for M^+–**L** complexes in methanol obtained by MD simulations. Data was binned at 0.1 Å and 5 ° interval, respectively.

3.2. Alkaline earth metal cations

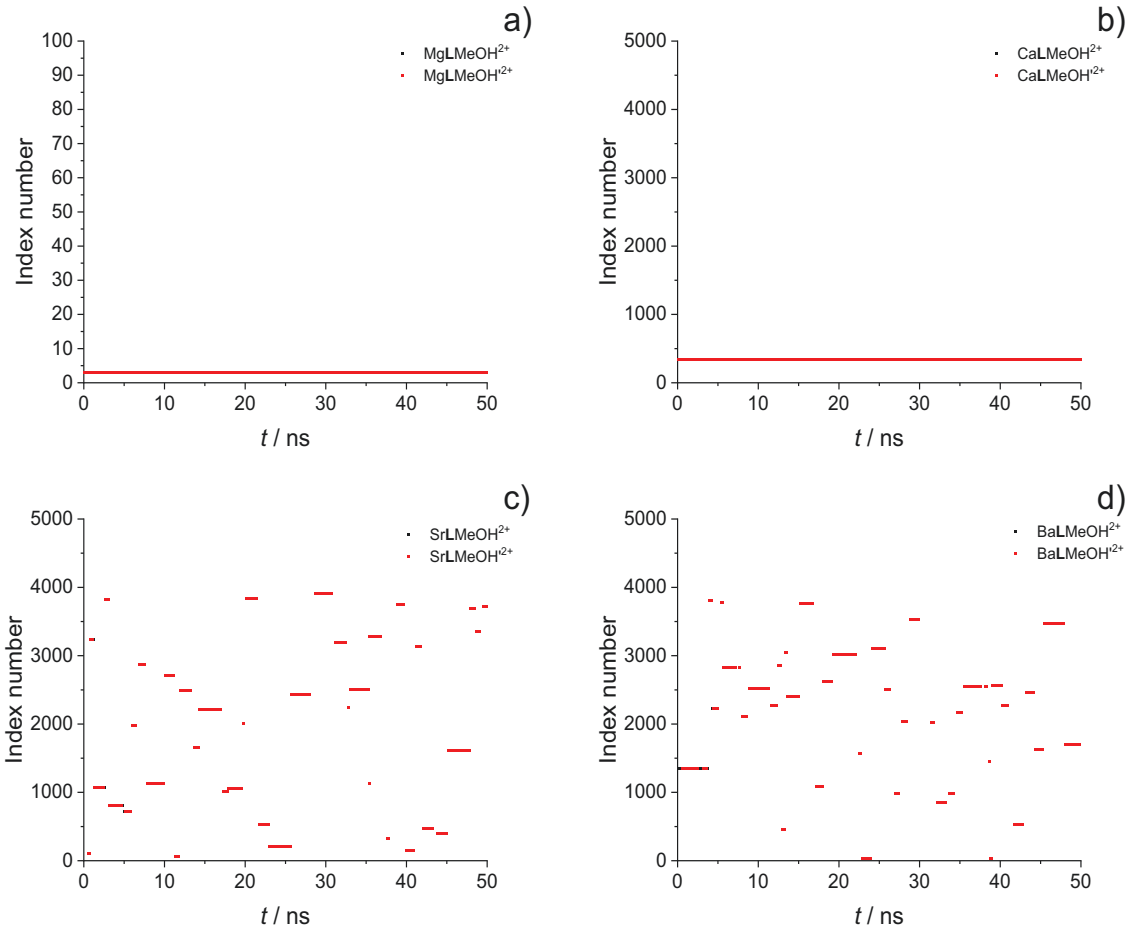

Figure S39. Index number of methanol that occupy hydrophobic cavities of a) Mg**L**MeOH^{2+} and Mg**L**MeOH'$^{2+}$, b) Ca**L**MeOH^{2+} and Ca**L**MeOH'$^{2+}$, c) Sr**L**MeOH^{2+} and Sr**L**MeOH'$^{2+}$, d) Ba**L**MeOH^{2+} and Ba**L**MeOH'$^{2+}$ during MD simulations in methanol at 25 °C.

Table S3. Energies of interactions of **L** with magnesium, calcium, strontium, and barium cations in methanol, occurrence time ratio of different chemical species, the number of ether, carbonyl, phenanthridine, and triazole groups which coordinate metal cations, and the structure of calixarene basket in the complexes obtained by MD simulations in methanol at 25 °C.

	Mg^{2+}		Ca^{2+}	
	Mg**L**$MeOH^{2+}$	Mg**L**$MeOH'^{2+}$	Ca**L**$MeOH^{2+}$	Ca**L**$MeOH'^{2+}$
$E(M^{2+}$–**L**) / kJ mol^{-1}	–1404	–1392	–1204	–1185
E(**L**–MeOH) / kJ mol^{-1}	–1567	–1549	–1620	–1596
E(**L**–$MeOH_{incl}$) / kJ mol^{-1}	–29	–13	–32	–14
$E(M^{2+}$–MeOH) / kJ mol^{-1}	–30	–62	–26	–61
$E(M^{2+}$–$MeOH_{incl}$) / kJ mol^{-1}	–2	–36	2	–35
t_{total} / ns	50		50	
t / t_{total}	0.010	0.990	0.014	0.986
N(coord., C–O–C)	4.00	4.00	3.63	3.86
N(coord., C=O)	2.00	2.00	1.99	1.84
N(coord., N_{phen})	0.04	0.00	0.18	0.00
N(coord., N_{triaz})	0.00	0.00	0.00	0.00
N($MeOH_{incl}$)	1	1	1	1
$\bar{d}$ / Å	8.16 7.99	8.10 7.98	8.12 7.90	8.03 7.91
σ(d) / Å	0.34 0.33	0.30 0.29	0.29 0.29	0.28 0.27
$\|d - d_{ref}\|$ / Å	0.38 0.29	0.32 0.25	0.32 0.24	0.27 0.22

	Sr^{2+}			Ba^{2+}		
	Sr**L**$MeOH^{2+}$	Sr**L**$MeOH'^{2+}$	Sr**L**$^{2+}$	Ba**L**$MeOH^{2+}$	Ba**L**$MeOH'^{2+}$	Ba**L**$^{2+}$
$E(M^{2+}$– **L**) / kJ mol^{-1}	–983	–978	–983	–993	–986	–993
E(**L**–MeOH) / kJ mol^{-1}	–1583	–1571	–1563	–1636	–1613	–1601
E(**L**–$MeOH_{incl}$) / kJ mol^{-1}	–57	–39	/	–56	–37	/
$E(M^{2+}$–MeOH) / kJ mol^{-1}	–34	–50	–38	–32	–49	–36
$E(M^{2+}$–$MeOH_{incl}$) / kJ mol^{-1}	5	–13	/	5	–14	/
t_{total} / ns					50	
t / t_{total}	0.591	0.225	0.184	0.613	0.232	0.155
N(coord., C–O–C)	3.75	3.62	2.99	2.99	3.34	3.05
N(coord., C=O)	1.36	1.40	1.50	1.50	1.44	1.48
N(coord., N_{phen})	0.76	0.92	1.20	1.20	0.98	1.15
N(coord., N_{triaz})	0.72	0.80	1.50	1.50	1.52	1.50
N($MeOH_{incl}$)	41	37	/	44	41	/
/ Å	8.06 7.76	0.83 7.76	8.22 7.36	8.07 7.77	8.02 7.78	8.26 7.31
σ(d) / Å	0.29 0.28	0.28 0.28	0.43 0.54	0.29 0.28	0.29 0.28	0.44 0.55
$\|d - d_{ref}\|$ / Å	0.28 0.23	0.26 0.23	0.47 0.57	0.30 0.24	0.27 0.23	0.50 0.62

$\bar{d}$ denotes average distance between opposing aryl carbon atoms connected to the *tert*-butyl groups and d_{ref} = 7.85 Å corresponds to C_{4v} *cone* conformation.

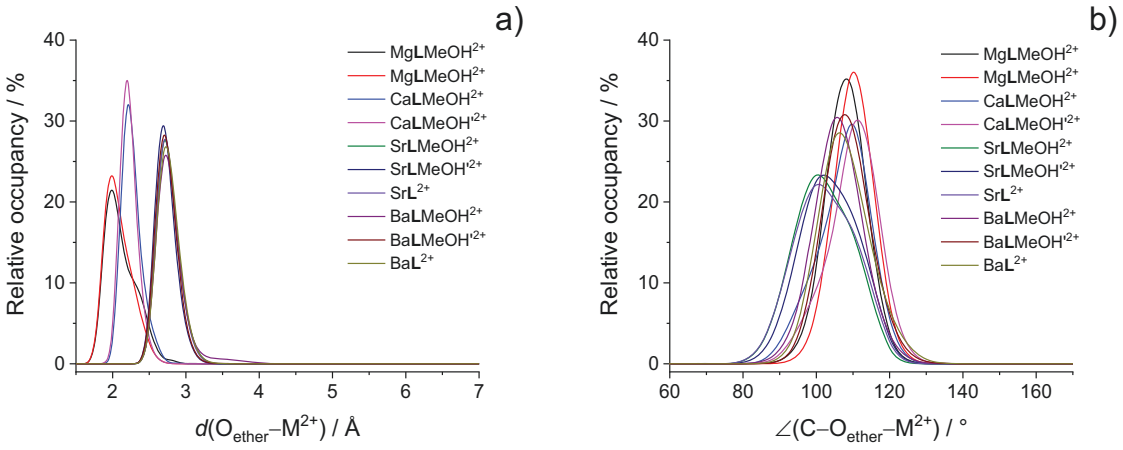

Figure S40. Distribution of a) metal cation–ether oxygen distances and b) metal cation–ether oxygen angles for M^{2+}–**L** complexes in methanol obtained by MD simulations. Data was binned at 0.1 Å and 5 ° interval, respectively.

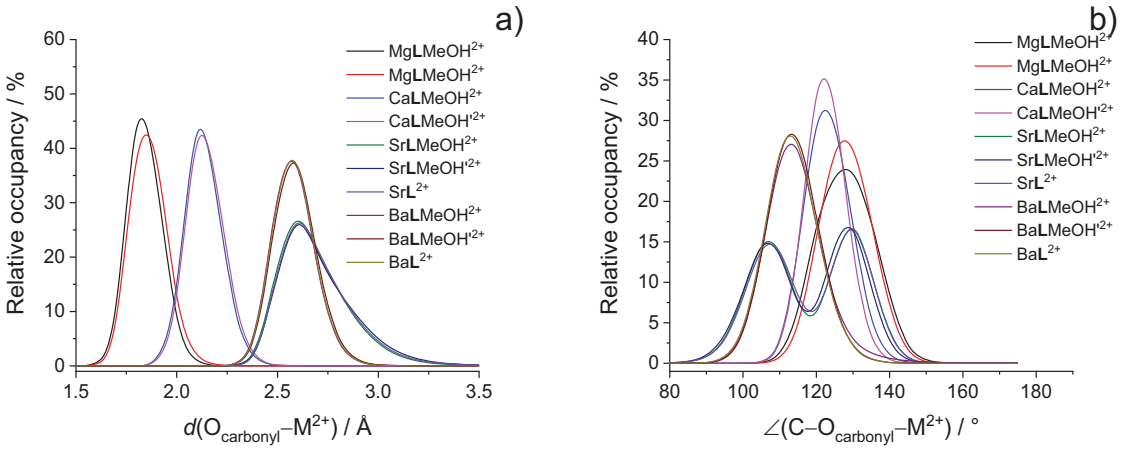

Figure S41. Distribution of a) metal cation–carbonyl oxygen distances and b) metal cation–carbonyl oxygen angles for M^{2+}–**L** complexes in methanol obtained by MD simulations. Data was binned at 0.1 Å and 5 ° interval, respectively.

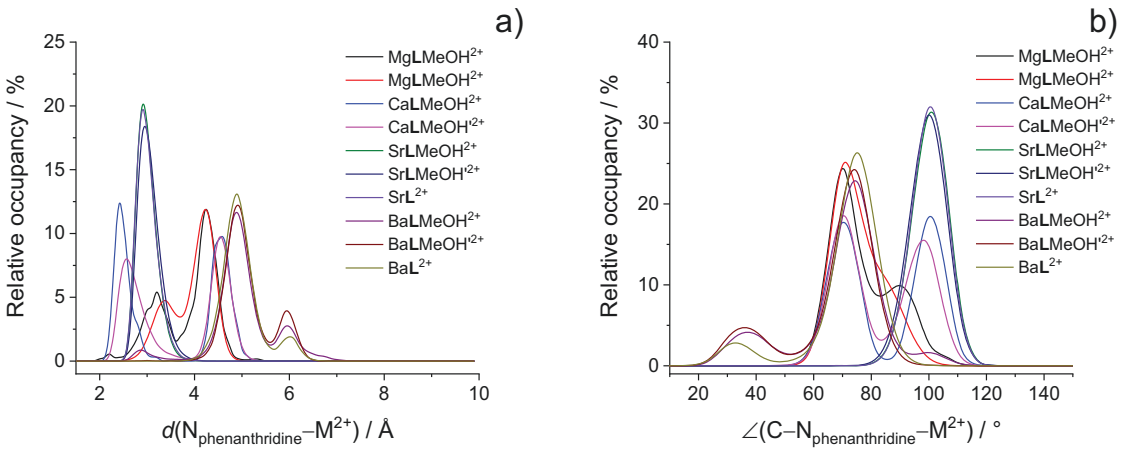

Figure S42. Distribution of a) metal cation–phenanthridine nitrogen distances and b) metal cation–phenanthridine nitrogen angles for M^{2+}–**L** complexes in methanol obtained by MD simulations. Data was binned at 0.1 Å and 5 ° interval, respectively.

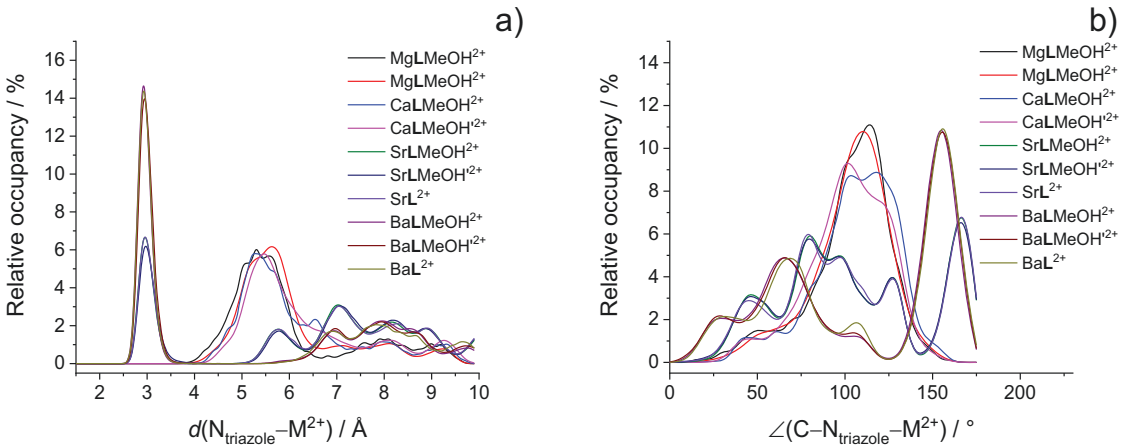

Figure S43. Distribution of a) metal cation–triazole nitrogen distances and b) metal cation–triazole nitrogen angles for M^{2+}–**L** complexes in methanol obtained by MD simulations. Data was binned at 0.1 Å and 5 ° interval, respectively.

Table S4. Gibbs energy, enthalpy, and entropy of solvation of alkali and alkaline earth metal cations and their ionic radii (coordination number 6).

Cation	$\Delta_{sol}G$ / kJ mol^{-1}	$\Delta_{sol}H$ / kJ mol^{-1}	$\Delta_{sol}S$ / J K^{-1} mol^{-1} [c]	r_{ion}(CN = 6) / pm [d]
Li^+	–486[a]	–550[a]	–214	76
Na^+	–376[a]	–439[a]	–212	102
K^+	–304[a]	–355[a]	–173	138
Rb^+	–279[a]	–327[a]	–161	152
Mg^{2+}	–1835[a]			72
Ca^{2+}	–1516[a]	–1655[b]	–467	100
Sr^{2+}	–1391[a]	–1524[b]	–446	118
Ba^{2+}	–1253[a]	–1393[a]	–468	135

[a] Y. Marcus, *Ions in Solution and their Solvation*, Wiley, Hoboken, **2015**.
[b] Y. Marcus, *Ion Properties*, M. Dekker, New York, **1997**.
[c] Values were calculated using $\Delta_{sol}S = (\Delta_{sol}H – \Delta_{sol}G)/T$
[d] *CRC Handbook of Chemistry and Physics, 95th edition*, (eds.: W. M. Haynes, D. R. Lide, T. J. Bruno), CRC Press, Boca Raton, **2014–2015**, pp. 12-11–12-12.
Solvation Gibbs energies and enthalpies were calculated as $\Delta_{hydr}X + \Delta_{tr}X(H_2O \rightarrow MeOH)$